https://doi.org/10.5194/egusphere-2022-384
Preprint. Discussion started: 9 June 2022
© Author(s) 2022. CC BY 4.0 License.

Eddy-covariance carbon fluxes of a heterogeneous forest: one tower - two heights

Alisa Krasnova[1,2], Dmitrii Krasnov[1], Hans Peter Ernst Cordey[1], Steffen M. Noe[1]

[1]Institute of Forestry and Engineering, Estonian University of Life Sciences, Estonia
[2]Institute of Science and Technology, University of Tartu, Estonia

Correspondence to: Alisa Krasnova (alisa.krasnova@emu.ee)

Abstract. Eddy-covariance (EC) is a widely used method for measuring ecosystem-scale fluxes of various gases. The sensor placement height is typically constrained by the canopy height and area of interest size. We studied the carbon dioxide fluxes over a hemiboreal mixed forest with two EC measurement systems located at 30 m and 70 m. The lower system NEE (NEE30) values were more positive (smaller sink or higher source) than the NEE of the higher one (NEE70), but this difference was prevalent in low light conditions and in May-November of all studied years. The nighttime and early morning difference (ΔNEE) increased with wind speed until ~2 m s^{-1} and friction velocity until ~0.35 m s^{-1} and linearly decreased after. ΔNEE was irregularly distributed over the wind direction sectors with high values overlapping the directions of South-East and South-West guy wire tunnels. Moreover, the shape of the NEE30 seasonal cycle was closer to that of a clear-cut area, and the difference between the systems increased with air temperature. The forest under study varied between a weak net sink and a strong net source on the annual scale. Directional heterogeneity correction shifted the annual NEE towards more negative values, but neither removed the difference between the systems nor changed the shape of the seasonal cycle. More studies are needed to assess the impact of clearcutting on the carbon accumulation under the measurement point.

1 Introduction

Carbon dioxide concentrations in the atmosphere featured a positive trend over the last century, with an increasing growth rate over the previous decade (Friedlingstein et al., 2019). During the same period, the terrestrial sink removed 33.7% of anthropogenic carbon dioxide from the atmosphere, with a large share attributed to forest ecosystems (Keenan and Williams, 2018). An increase in NEP and GPP of 1% annually has been recently reported based on the flux time series of 23 forests in Europe and the USA (Fernández-Martínez et al., 2017). Forests play an essential role in the climate systems, being a part of large-scale feedback between atmospheric and biospheric processes (Lappalainen et al., 2016). The capacity of forests to interact with aerosols and clouds via a carbon-driven feedback loop (Ezhova et al., 2018; Kulmala et al., 2014) puts them into focus for climate mitigation strategies and sustainable resource development. The variety of forest management practices, wood harvesting, and forests degradation due to the human impact add to the global CO_2 budgets on the emission side (Friedlingstein et al., 2019; Noormets et al., 2015).

https://doi.org/10.5194/egusphere-2022-384
Preprint. Discussion started: 9 June 2022
© Author(s) 2022. CC BY 4.0 License.

Hemiboreal mixed forests are located in a transitional zone between boreal and temperate ecosystems bearing the features of both (Ahti et al., 1968; European research agency, 2016). The mixture of different dominating tree species of varying age and the additional spatial variability introduced by forest management activities such as thinning and clearcutting form a highly heterogeneous forest landscape. Clear-cut harvesting leads to abrupt changes in canopy height and alters, therefore, the vertical shape and source/sink capacity of the forest.

Over the last decades, the eddy-covariance method (EC) has been widely used to calculate CO_2 fluxes on the ecosystem scale (Baldocchi, 2014). When placing an EC system, one has to consider different factors, including the area of interest size, canopy height, and landscape topography (Burba, 2013). The EC system has to be placed high enough to be in a well-mixed air layer above the ecosystem of interest and to avoid the effect of canopy roughness (Munger et al., 2012). If the measurement height is too close to the canopy flux values can be exposed to local effects introducing a location bias, a degree to which the certain measured fluxes differ from the aggregated ecosystem-scale flux (Rebmann et al., 2018; Schmid and Lloyd, 1999). On the other hand, if an EC system is placed too high over the canopy, the ecosystem of interest might be underrepresented in the footprint area of the tower in all the wind directions.

To study the exchange of CO_2 between a heterogeneous forest ecosystem and the atmosphere, the atmospheric tower of the SMEAR Estonia (Station for Measurement ecosystem atmosphere relations) (Noe et al., 2015) was equipped with two identical EC systems placed at 30 and 70 m height, 10 m and 50 m in average above the canopy respectively. According to Munger et al. (2012), the recommended measurement height over the forested ecosystems can be calculated as:

$$h_m \approx d + 4(h_c - d)$$

where h_m - measurement height; h_c - mean canopy height; d - zero plane displacement height (approximately equal to 0.67 of canopy height). Thus, the recommended EC measurement height for SMEAR Estonia would be 39.8 m.

According to somewhat more relaxed pan-European research infrastructure ICOS (Integrated Carbon Observation System) requirements, the measurement height for forested or more structurally complex ecosystems is recommended to be between $1.67h_c$ and $2h_c$, resulting in 33.4 m – 40 m for our tower (Rebmann et al., 2018). The EC measurements done at the height of more than $2h_c$ were previously used to estimate the carbon balance of an entire landscape over the agricultural area (Soegaard, 2003), mixed agricultural and forest landscape (Barcza et al., 2020; Haszpra et al., 2005), land-water mosaic (Sogachev and Dellwik, 2017), and boreal landscape (Chi et al., 2020, 2019).

This study aimed to analyse the differences in CO_2 fluxes measured with EC systems mounted on the same tower but at two different heights above the canopy over a heterogeneous mixed hemiboreal forest. We hypothesise that the EC system located closer to the canopy will detect local features while the higher positioned system will detect naturally integrated CO_2 flux.

https://doi.org/10.5194/egusphere-2022-384
Preprint. Discussion started: 9 June 2022
© Author(s) 2022. CC BY 4.0 License.

2. Methods

2.1 Site and instrumentation

SMEAR Estonia was established in 2014 at the Järvselja Experimental Forestry Centre (58°16'N, 27°18'E) to measure the exchange of energy and matter in the atmosphere-biosphere system (Noe et al., 2015). The forest ecosystem at the study site is typical for the area and is represented by a mosaic of managed forested compartments dominated by Scots pine (*Pinus sylvestris* L.), Norway spruce (*Picea abies* (L.) Karst.), and birch species (*Betula pendula* Roth and *Betula pubescens* Ehrh.). Several clear-cut areas of various sizes and ages and non-managed old-growth forest areas are also located within the tower footprint (Fig. 2). In particular, during the tower installation in 2013/2014 three areas were deforested in the North, South-East and South-West directions to accommodate the tower guy wires. The average height of the forest stand is 20 m; the stand age varies greatly and, in some cases, reaches up to 150 years for managed stands and older than 100 years in the case of the non-managed protected old-growth forest. The main soil type is Haplic Gleysol (eutric), with a thick humus horizon in wetter places. A more detailed site description can be found in Noe et al. (2015, 2011).

Ecosystem CO_2 flux was measured with two identical eddy-covariance systems (EC30 and EC70) installed in 2014 on a 130 m atmospheric tower at 30 and 70 m height. The systems were mounted on 6 m long booms reaching 4 m away from the tower structure to the major wind direction. Both systems consist of a fast 3D sonic anemometer (uSonic Class A, Metek GmbH, Germany) and an enclosed gas-analyser (LI-7200, LI-COR Inc., NE, USA) measuring CO_2 and H_2O concentrations at a frequency of 10Hz. Additionally, 3D sonic anemometers of the same model were installed at 50, 90, and 110 m to assess the features of the wind profile. Here we present four years of measurements (2015-2018) covering a wide variety of weather conditions. Data from 2014 was discarded because the deployment of a piping system for profile measurements on the tower disturbed a significant portion of measurements.

According to dominating tree species, three sample plots were chosen around the tower to estimate forest floor respiration (Fig. 2). The efflux of CO_2 was measured with a transparent non-steady-state flow manual chamber. The 7L chamber was equipped with Vaisala GMP343 (Vaisala Oyj, Finland) infrared gas-analyser, Vaisala HM70 (Vaisala Oyj, Finland) humidity meter, and a small fan for mixing the air inside the chamber. Nine stainless steel collars with a basal area of 0.073 m^2 were installed per sample plot. Respiration measurements were done weekly during the snow-free period starting the year 2016. Soil chamber enclosure time was 5 minutes, out of which 2 minutes were used for the flux calculation. The first minute of measurements was considered stabilisation time and not used in the analysis.

Meteorological measurements (air temperature, relative humidity, rain detection) were provided by Vaisala Weather transmitter WXT520 systems (Vaisala Oyj, Finland). Total incoming solar radiation was measured using Delta-T SPN1 sunshine pyranometer (Delta-T Devices Ltd., UK). Soil moisture and temperature were measured with ML3 sensors connected to Delta-T DLe2 data-logger (Delta-T Devices Ltd., UK). Soil sensors were placed at 10 cm depth, and measurements were done with 5 minutes frequency.

https://doi.org/10.5194/egusphere-2022-384
Preprint. Discussion started: 9 June 2022
© Author(s) 2022. CC BY 4.0 License.

2.2 Data analysis

Both EC30 and EC70 systems flux calculation followed precisely the same procedure. Half-hourly fluxes of CO_2 were calculated as a covariance of vertical wind speed and CO_2 concentration using software EddyUH developed by Helsinki university (Mammarella et al., 2016). Raw data processing included de-spiking (Vickers and Mahrt, 1997) and block averaging. Planar fit (Wilczak et al., 2001) was chosen for the rotation of the three wind components due to the complex structure of the heterogeneous forest. Time lag optimisation was performed using the covariance maximisation approach. Low- and high-frequency spectral corrections (Moncrieff et al., 2005, 1997) were applied. Further data analysis was performed using MATLAB (ver. 2016a-2018b, Mathworks Inc.), ReddyProcWeb online software (Wutzler et al., 2018) and Mathematica (ver. 11-12, Wolfram Inc.). A moving point test for the friction velocity (u*) threshold estimation (Papale et al., 2006) was performed over the nighttime data (Rg<15 W m^{-2}). The estimated u* threshold value of 0.43 ms^{-1} would result in the removal of 58% of all the nighttime fluxes of EC30 and 60% of all the EC70 nighttime fluxes. To avoid this massive loss of data, we decided to use a 0.3 ms^{-1} friction velocity threshold, as has been previously utilised for other northern forest ecosystems (Lindroth et al., 2020, 2018). Daytime values were not subjected to the same friction velocity filtering procedure due to the absence of obvious influence in the visual inspection.

Following the micrometeorological sign convention, negative values of net ecosystem exchange (NEE) denote a flux from the atmosphere into the ecosystem, while positive values mean CO_2 release. To study the differences in diurnal cycles and the influence of wind direction, quality controlled NEE of all four years was pooled together and split into four seasons according to plant physiological activity in the given climate rather than calendar seasons: November to February represent the dormancy period, March to April is the spring transitional period, May to August is considered as the active vegetation season, September to October is the autumn transitional period.

The difference between the half-hourly fluxes of the two systems (ΔNEE) was calculated as ΔNEE=NEE30-NEE70. The ΔNEE values above zero indicate that NEE30 is more positive than NEE70, while the negative ΔNEE denotes the opposite.

To assess the influence of footprint heterogeneity on the fluxes, it is possible to split the data according to wind direction sectors. The issue arises as the data of a particular wind direction sector can be dominated by certain meteorological conditions or times of the day or season, overshadowing the footprint effect. To decrease this possibility, we pooled together May-September NEE (not gap-filled) and analysed light-response curve parameters (Michaelis-Menten equation, eq. 1) for daytime NEE and Lloyd & Taylor equation (eq. 2) reference respiration for the nighttime NEE for each 5-degree wind direction sector. The activation energy (E_0) of the Lloyd & Taylor model was determined for the whole dataset to ensure the fit.

$$\mathrm{NEE} = \frac{\alpha R_g \mathrm{GPP_{max}}}{\alpha R_g + \mathrm{GPP_{max}}} + \mathrm{ER_{day}}, \quad (1)$$

where α (µmol C J^{-1}) is light use efficiency (ecosystem quantum yield), Rg (Wm^{-2}) is global radiation, GPP_{max} (µmol C m^{-2} s^{-1}) is the maximum GPP under given conditions, RE_{day} (µmol C m^{-2} s^{-1}) is the daytime respiration.

https://doi.org/10.5194/egusphere-2022-384
Preprint. Discussion started: 9 June 2022
© Author(s) 2022. CC BY 4.0 License.

$$\mathrm{ER} = R_{\mathrm{ref}} \mathrm{e}^{E_0\left(\frac{1}{\mathrm{T_{ref}}-T_0}\right)-\left(\frac{1}{T-T_0}\right)}, \quad (2)$$

where R_{ref} (µmol C m^{-2} s^{-1}) is the respiration at the reference temperature; E_0 (kJ mol^{-1}) is the activation energy; T (°C) is the measured air temperature. T_{ref} was set to 15 °C, and T_0 was kept constant at −46.02°C as in Lloyd and Taylor (1994).

To calculate the sums at different time scales, gaps in the data were filled using marginal distribution sampling (MDS) (Reichstein et al., 2005) implemented in ReddyProcWeb. MDS method is a combination of look-up tables and average diurnal variation. The latter is applied when there are not enough measurements to compile a look-up table (a more detailed description of the gap-filling algorithm can be found in Wutzler et al., 2018). Look-up tables are based on the assumption that fluxes under a combination of similar meteorological parameters (solar radiation, air temperature, and vapour pressure deficit) and within a certain time window are similar, irrespective of the footprint part they originate from. While this approach is adequate for the homogeneous terrain, the input of the possible "hot spots" and irregularities in the footprint area can be over- or underestimated in the total budget. Moreover, the non-uniform distribution of wind directions can lead to an overrepresentation of some parts of the footprint area. If such a dominating wind direction sector coincides with flux "hot spots", their combined influence will add up to the bias. Hadden and Grelle (2017) suggested a weighted correction that can be applied to measured NEE values to account for directional heterogeneity. We performed this correction, splitting the NEE data into four seasons (as described above), night and day values separately (Rg threshold 5 W m^{-2}). Each period was further divided according to wind directions (8 sectors, 45°). For each NEE within the subset, the correction was performed as follows:

$$\mathrm{NEE_{corrected}} = \mathrm{NEE_{measured}} \frac{N_{\mathrm{total}}}{8N_{\mathrm{ws}}} \quad (3)$$

where N_{total} is the total number of measurements and N_{ws} is the number of measurements in the given wind sector.

To test the sensitivity of the correction, we additionally estimated the correction multipliers for the angular width of 24°, 30°, 36°, 60° and 90° wind sectors and performed gap-filling for every option.

The Kruskal-Wallis test with Bonferroni adjustment was performed to assess the statistical significance of the differences between the two systems and the influence of the wind sector size choice in directional heterogeneity correction. The impact of the correction was tested using Wilcoxon signed-rank test before and after the gap-filling.

To get the estimates of gross primary production (GPP) and ecosystem respiration (ER), flux partitioning was performed in the ReddyProcWeb tool. The daytime data-based approach (Lasslop et al., 2010) was chosen over the more widely used nighttime data-based one to obtain the ER estimated independently from the nighttime measurements.

The footprint area was estimated with the Kljun 2D footprint model using the FFPonline tool (Kljun et al., 2015). Friction velocity filtered data were similarly split into seasons as in other analyses; all four years were pooled together.

The forest floor respiration was calculated from the rate of CO_2 concentration change in the chamber using the following equation:

$$F = \frac{\Delta C}{\Delta t} h \quad (4)$$

https://doi.org/10.5194/egusphere-2022-384
Preprint. Discussion started: 9 June 2022
© Author(s) 2022. CC BY 4.0 License.

where C denotes the concentration in ppm, t – is time in hours, h =V/A denotes the effective chamber height, V and A denote chamber volume and cross-sectional area, respectively.

3. Results

3.1 Meteorological conditions

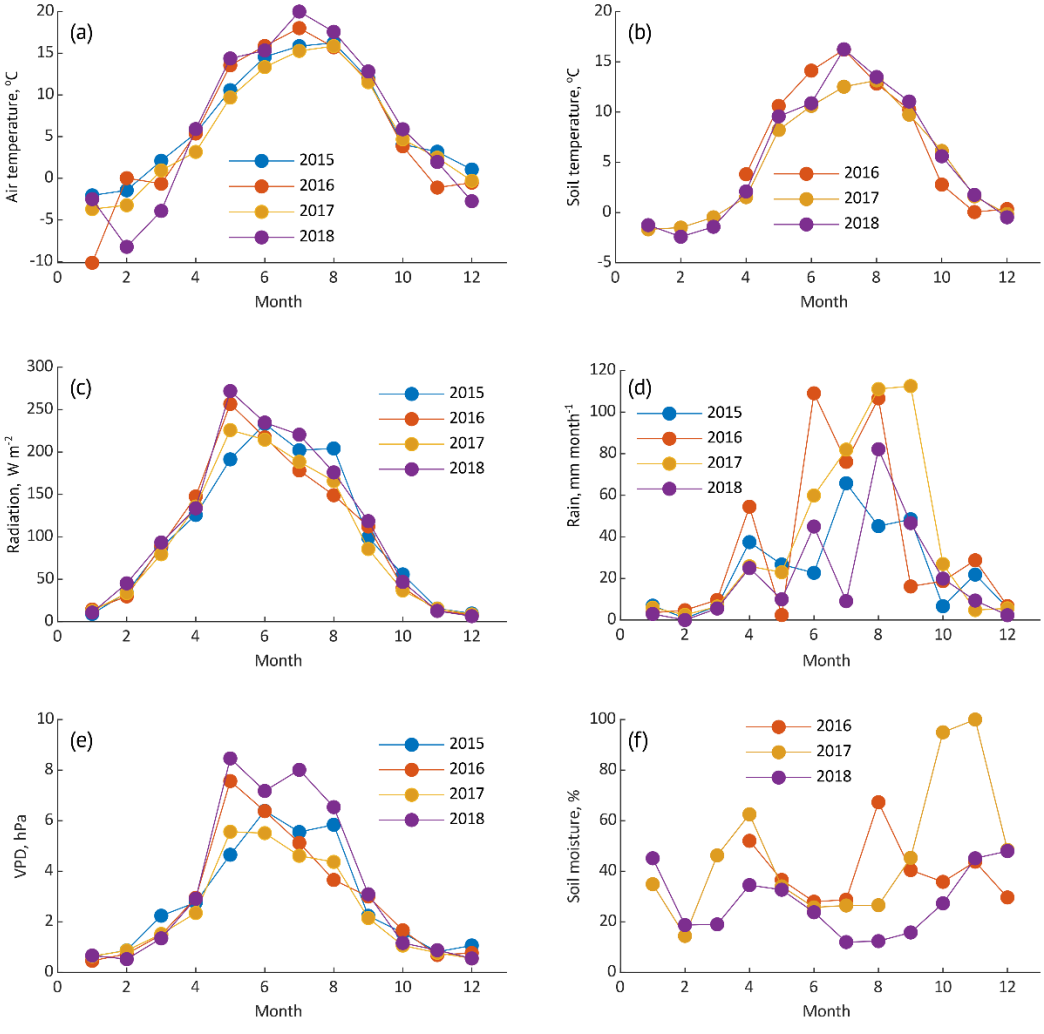

Fig. 1 Monthly means of air temperature (A), soil temperature (B), global radiation (C), montly sums of rain (D), means of vapour pressure deficit (E) and soil moisture (F) during the 2015-2018.

Table 1. Annual means ± standard deviations of meteorological parameters during the study years. Rain values are given as yearly sums.

https://doi.org/10.5194/egusphere-2022-384
Preprint. Discussion started: 9 June 2022
© Author(s) 2022. CC BY 4.0 License.

	Tair, °C	Rg daytime, W m^{-2}	VPD, hPa	Rain, mm	SWC, %	Tsoil, °C
2015	7.4 ± 7.6	195.6 ± 201.4	2.9 ± 3.8	295	-	-
2016	6.1 ± 9.7	207.9 ± 215.4	2.9 ± 3.9	437	-	-
2017	5.4 ± 8.0	199.5 ± 208.3	2.6 ± 3.4	467	48.8 ± 33.1	5.0 ± 6.2
2018	6.3 ± 10.3	228.4 ± 228.6	3.5 ± 5.1	258	36.7 ±29.0	4.2 ± 7.0

The meteorological conditions of the four studied years are summarised in Fig. 1 and Table 1. Overall, 2015 had a mild winter and higher air temperatures in the late summer with decreased amounts of rain, leading to the highest average annual mean temperature of the studied years. The year 2016 can be nominated as "the average year" in our ensemble. The year 2017 was characterised by the coldest growing season with the lowest temperatures from April to September. Exceptionally high amounts of rain in July-September 2017 resulted in an elevation in soil water content that persisted throughout the autumn. The vapour pressure deficit (VPD) was significantly lower in 2017, even during warmer periods if compared to other years. In 2018, the heatwave over Europe resulted in a very dry July and the second-highest annual average temperature. The global radiation (Rg) peaked in May 2016-2018, but in 2015 the highest solar radiation was measured in June. That matches the long-term climatic data of Estonia (http://www.ilmateenistus.ee/kliima/kliimanormid/pilvisus/?lang=en), where the lowest amount of cloud cover is during May, which is among the three months with the most sunshine hours per month.

3.2 Footprint area and wind field pattern

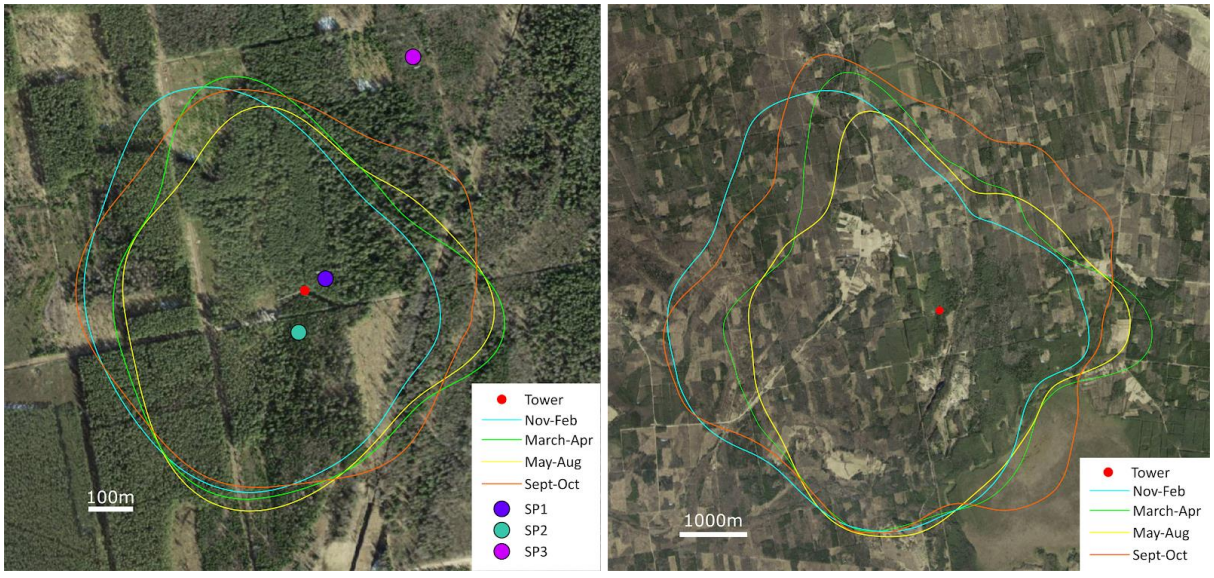

Fig. 2. Flux footprint climatology of EC30 (left panel) and EC70 (right panel) estimated using FFPonline tool (Kljun et al., 2015). The seasons' data were pooled over the four studied years (2015-2018). Contour lines represent the area where the cumulated flux

https://doi.org/10.5194/egusphere-2022-384
Preprint. Discussion started: 9 June 2022
© Author(s) 2022. CC BY 4.0 License.

footprint function reaches 90%; colours denote different periods. The coloured rounds (SP1, SP2, SP3) mark the location of sample plots for forest floor respiration measurements. Map source: X-GIS. Estonian Land Board. All rights reserved.

The footprint area was 0.58±0.04 km^2 for EC30 and 25.97±3.57 km^2 for EC70 (Fig. 2). There are slight differences in the shape of the footprint areas in different seasons throughout the year, especially in the North-West and eastern directions. The majority of the EC30 footprint area is covered with coniferous forests (dark green in Fig. 2, left panel); several clear-cuts of different ages are present. Within the much larger EC70 footprint area, a mosaic of coniferous (dark green) and deciduous (brown) species dominates the forested compartments. Additionally, clear-cuts, roads and three small villages: Agali (19 residents) to the North-West, Järvselja (35 residents) to the South-East, and Liispõllu (11 residents) to the South West from the tower (population numbers are from 2017), are also within the footprint adding to the spatial heterogeneity of the area.

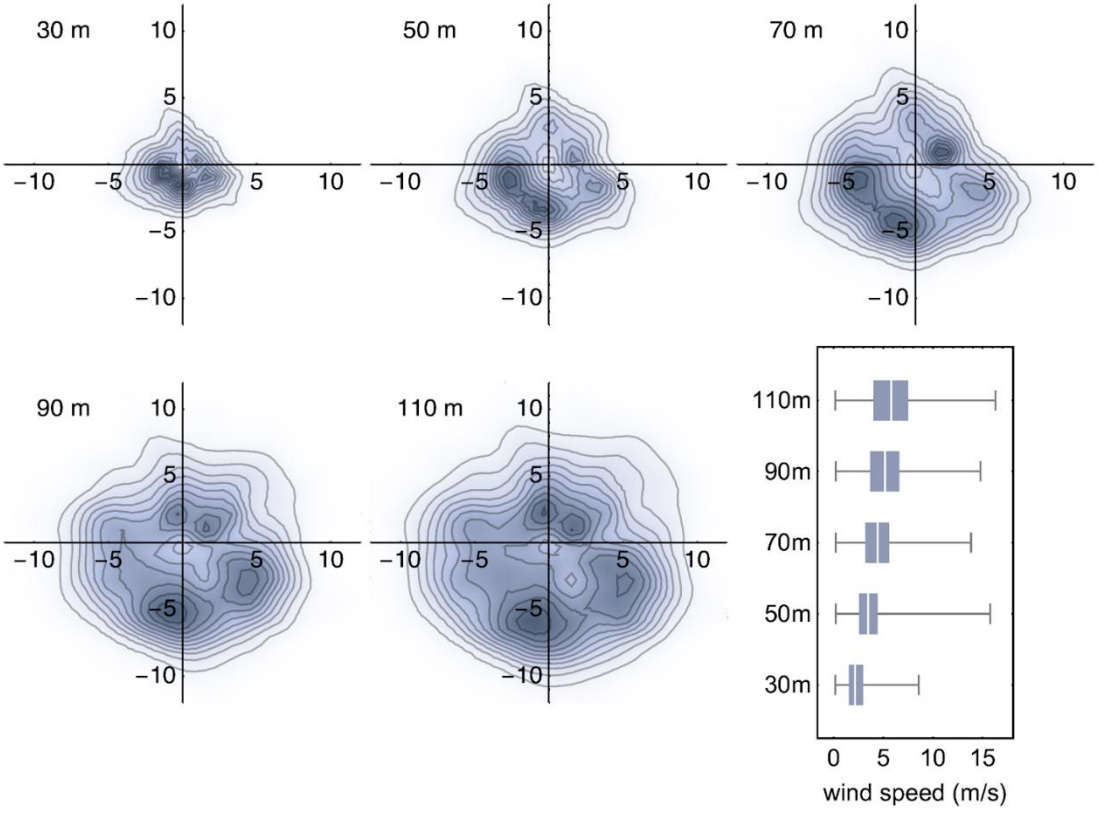

Fig. 3. Horizontal wind profile measured on five heights at the atmospheric mast in Järvselja. Data are half-hourly medians and cover the time from January 2015 until December 2018. The x and y-axis on the contour plots are the wind speed in m s^{-1} and the darker colour denotes a higher density in the wind direction and allows visualising the major wind directions for each sensor height. The Box-Whisker chart in the lower panel shows the median wind speed profile over the mast.

The median vertical wind speed measured at different heights of the tower followed the expected logarithmic profile (Fig. 3). Wind directions for lower heights follow the pattern reported by Jaagus and Kull (2011), where western and south-western

https://doi.org/10.5194/egusphere-2022-384
Preprint. Discussion started: 9 June 2022
© Author(s) 2022. CC BY 4.0 License.

wind directions prevail. However, a wind field is turned to some degrees counter clockwise the higher the measurement is located, and the easterly wind directions strengthen from 70 m and higher. The shape of the wind density field at 30m height has a weak similarity with a triangular pattern, especially during the vegetation period (Fig. 4). At 70 m height, this triangular pattern is almost diminished, and a circular pattern prevails on the levels above.

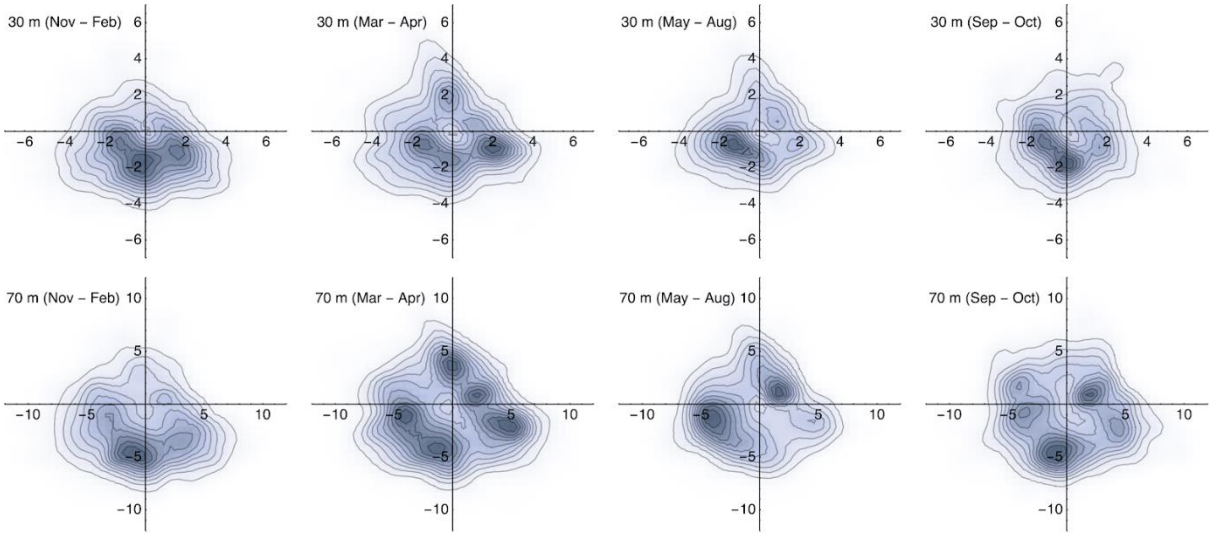

Fig. 4. Comparison of the local horizontal wind field pattern on 30 m and 70 m for different seasonal time intervals. Please note that axis scaling was chosen to allow the best visible comparison between 30 and 70 m and the ranges are different.

Horizontal wind field patterns of EC30 and EC70 varied over the season (Fig. 4). During the dormancy period (November-February), southern winds prevailed. In spring (March-April), the EC30 wind field was similar to the dormancy period, while EC70 featured a distinctive bidirectional pattern. South-East wind direction dominated during vegetation season and autumn months for EC30, while a high share of north-east winds was additionally present at EC70.

https://doi.org/10.5194/egusphere-2022-384
Preprint. Discussion started: 9 June 2022
© Author(s) 2022. CC BY 4.0 License.

3.2 Half-hourly fluxes and diurnal cycles comparison

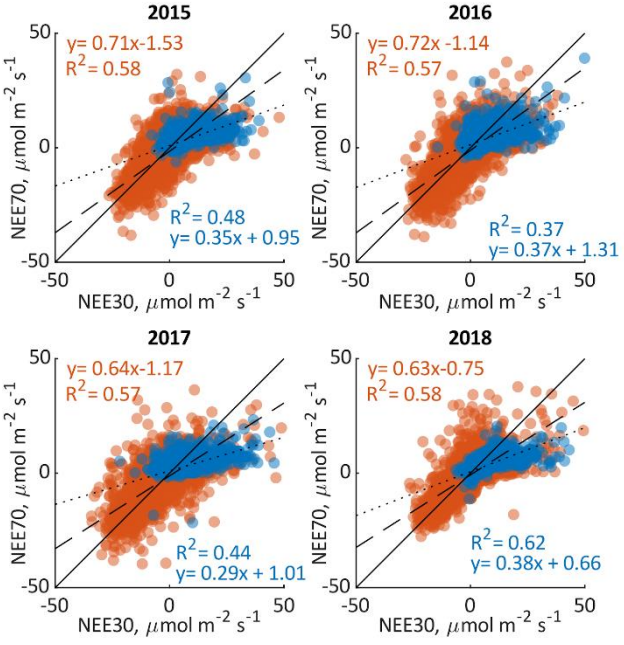

Fig. 5. Measured (not gap-filled) half-hourly averaged NEE values from 30m (NEE30) and 70m (NEE70) EC systems. Blue circles correspond to nighttime (Rg<5 W m^{-2}), and red circles are daytime values. The solid line is 1:1 line, the dashed line is a linear fit for the daytime values, and the dotted line is a linear fit for the nighttime values.

The relation between fluxes measured from the two heights is shown in Fig. 5. All four studied years have a similar pattern on a half-hourly scale, with negative daytime fluxes being closer to the 1:1 line and positive nighttime (and some of the daytime) NEE30 being consistently higher than NEE70. The slopes of the daytime measured NEE are below 1 and for nighttime NEE measurements below 0.5. The slopes of daytime NEE were similar in 2015 and 2016 (0.71 and 0.72, respectively) and slightly smaller but similar in 2017 and 2018 (0.64 and 0.63, respectively). For nighttime measurements, the slope in 2017 was the lowest (0.29), while similar slopes were obtained in the other three years of the study (0.35-0.38).

https://doi.org/10.5194/egusphere-2022-384
Preprint. Discussion started: 9 June 2022
© Author(s) 2022. CC BY 4.0 License.

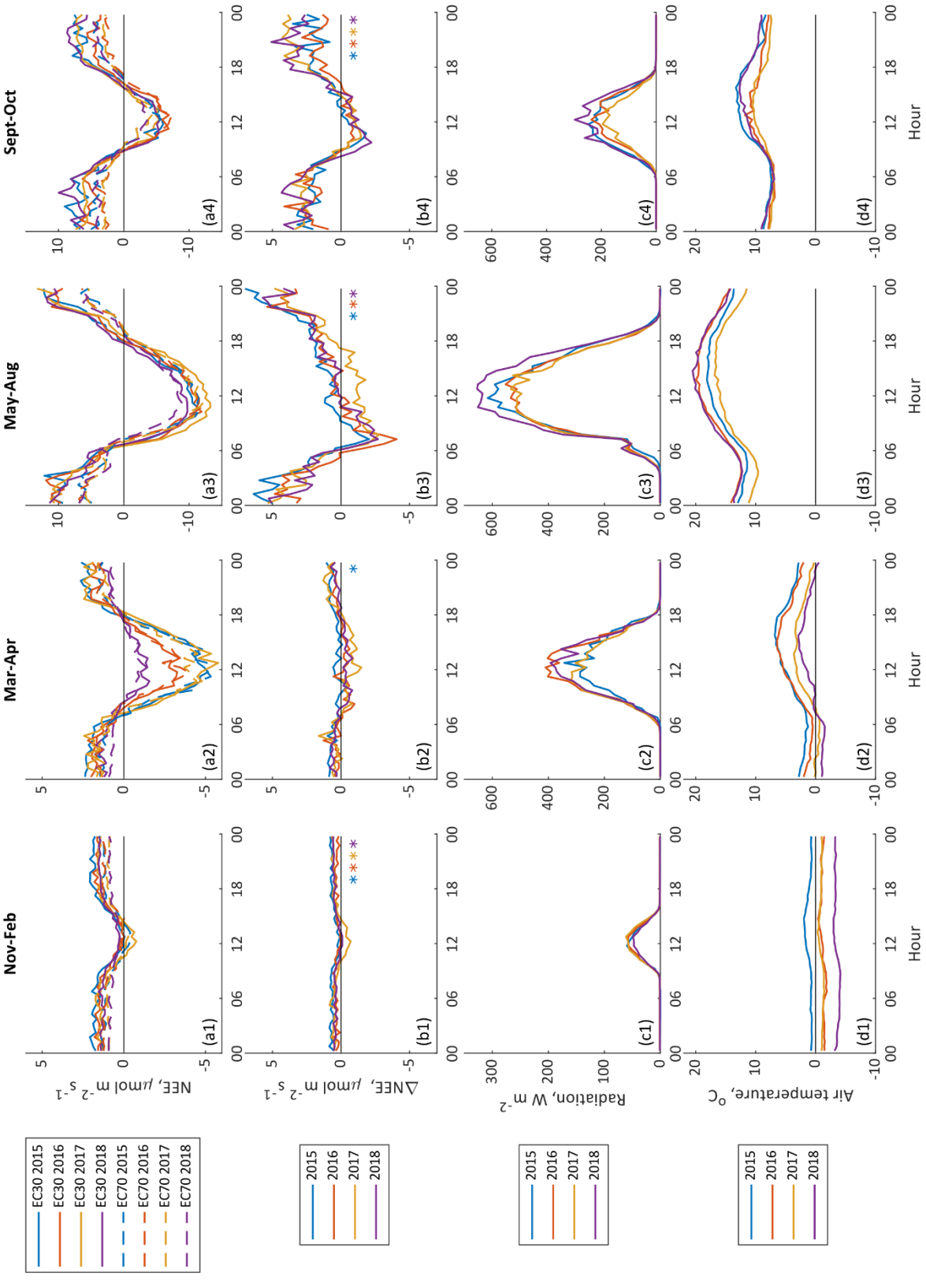

https://doi.org/10.5194/egusphere-2022-384
Preprint. Discussion started: 9 June 2022
© Author(s) 2022. CC BY 4.0 License.

Fig. 6. Median diurnal cycle of NEE from EC30 (solid lines) and EC70 (dashed lines) in different seasons of four studied years (panels a1-a4) and corresponding diurnal cycles of median differences between the NEE (ΔNEE = NEE30-NEE70) of two systems in different years (panels b1-b4). Asterisks on the panels b1-b4 stand for significant difference (Bonferroni corrected p<0.05) between the NEE30 and NEE70 within the given year and season according to Kruskal-Wallis sign-rank test. Colour denotes the year and corresponds to the colour of the line. Median diurnal cycles of solar radiation and air temperature (panels c1-c4 and d1-d4). The difference of scales for different panels is kept to see the difference between the years.

Diurnal variations of both NEE30 and NEE70 followed the same pattern, with negative values (carbon sequestration) in the presence of solar radiation and positive values (carbon release) during the nighttime (Fig. 6). Comparing the two systems, we found that NEE30 was consistently higher at low solar radiation while the daytime difference was close to zero or slightly negative. This difference observed in all the studied years was most pronounced in May-August and slightly weaker in autumn (September – October). The median difference (and interquartile range) between the measured NEE values at 30 min intervals was 0.37 (-0.25 to 1.05), 0.14 (-1.05 to 1.08), 0.80 (-1.76 to 3.88), 0.85 (-0.90 to 3.26) μmol m^{-2} s^{-1} for the four periods, respectively. The difference was significant (p<0.0001) during the dormancy period and autumn transitional period in all the years. In spring, it was significant only in 2015 and in the vegetation period for all the years except 2017.

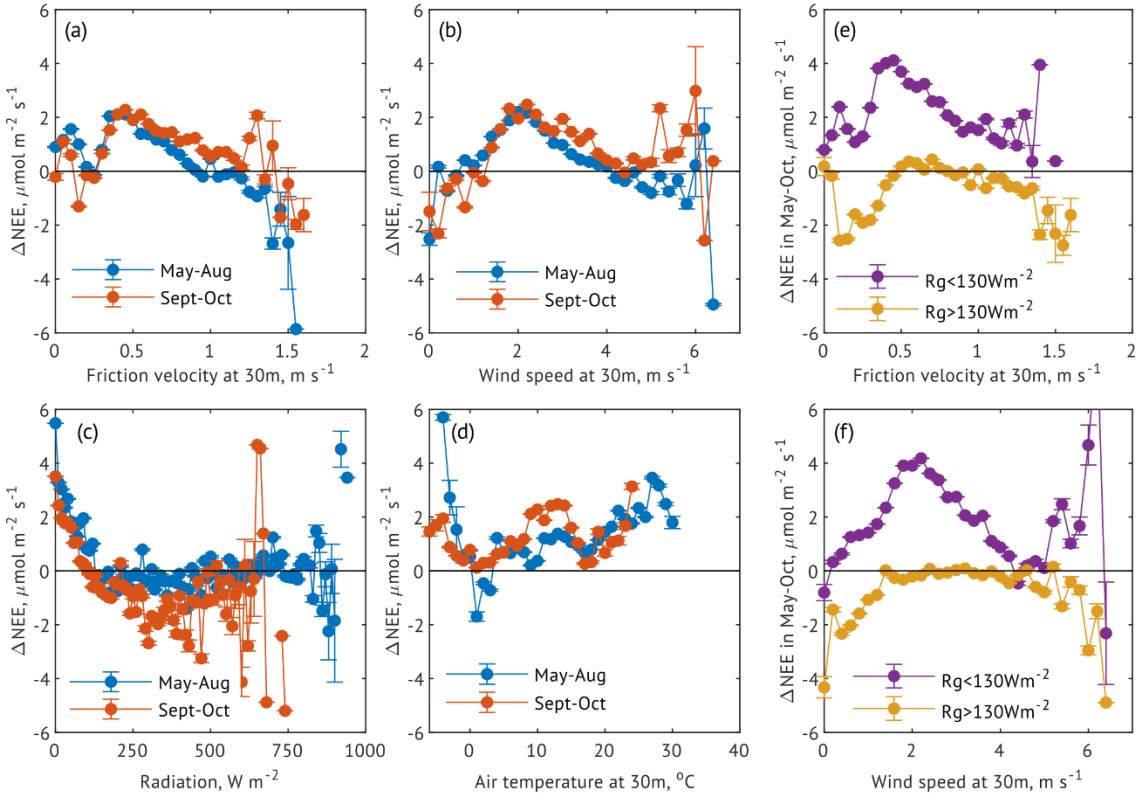

Fig. 7. Bin-averaged half-hourly ΔNEE (NEE30-NEE70) against friction velocity (A, E), wind speed (B, F), radiation (C) and air temperature (D) in summer (May-August) and autumn (September-October) months (A-D) and at different radiation levels (E-F). The data from 2015-2018 were pooled together. The markers are the averages of 0.05 m s^{-1} for the friction velocity (A, E), 0.2 m s^{-1} for the wind speed (B, F), 10 W m^{-2} for the radiation (C), 1 °C for the air temperature (D). The error bars denote the standard errors of the bin averages.

https://doi.org/10.5194/egusphere-2022-384
Preprint. Discussion started: 9 June 2022
© Author(s) 2022. CC BY 4.0 License.

We assessed the influence of wind speed, friction velocity (u*), air temperature and radiation on the difference between the measured half-hourly NEE (ΔNEE=NEE30-NEE70) in May-August and September-October, all four years pooled together (Fig. 7a-d). ΔNEE is above zero in the cases when NEE30 is more positive than NEE70, while ΔNEE below zero marks the opposite. ΔNEE was the highest at u* 0.4 m s^{-1} and was steadily declining with the increase of the friction velocity values (Fig. 7a). ΔNEE was increasing with the wind speed until around 2 ms^{-1} and steadily decreased after it (Fig. 7b). The difference between the two systems decreased with the increase of radiation until Rg~200 W m^{-2} with no further effect at higher radiation values (Fig. 7c). ΔNEE was primarily positive until the radiation reached around 130 W m^{-2}. In May-August, the difference between the two systems increased with air temperature values higher than 5 °C. (Fig. 7d).

Additionally, we studied the influence of wind speed and friction velocity on May-October ΔNEE above and below the estimated radiation threshold of 130 W m^{-2} (Fig. 7e-f). ΔNEE was increasing until a distinctive peak of around u* 0.35 m s^{-1} in the low light conditions, and u* 0.55 m s^{-1} for the higher radiation values. After passing the peak value, the difference steadily decreased with the increase of u*. Similar pattern was observed for wind speed with the peaks at 2 m s^{-1} and 1.4 m s^{-1} for lower and higher light conditions, respectively. At the Rg>130 W m^{-2} the increase of wind speed after 1.4 m s^{-1} had no influence on the ΔNEE and the difference between the systems was close to zero. It has to be noted that the low friction velocity (<0.3 m s^{-1}) nighttime (Rg<15 W m^{-2}) values were removed from both NEE30 and NEE70 in the course of the u* filtering.

In the absence of sufficient light, nighttime NEE represents ecosystem respiration (ER). If the difference between the two systems is caused by higher ER values coming from the EC30 footprint area, then the same difference should also be observed during the daytime. Flux partitioning was performed utilising the daytime method (Lasslop et al., 2010), thus minimising the impact of already observed nighttime differences on the daytime ER estimates.

Indeed, we found ER30 to be higher than ER70 for both nighttime (measured) and daytime (modelled) periods (Fig. 8). The difference was most evident in the summer and autumn months. While ER70 was higher than ER30 in the dormancy period and March-April of 2016, the difference between the daily sums was not significant (Table A1). No significant difference was also observed for March-Apr 2017.

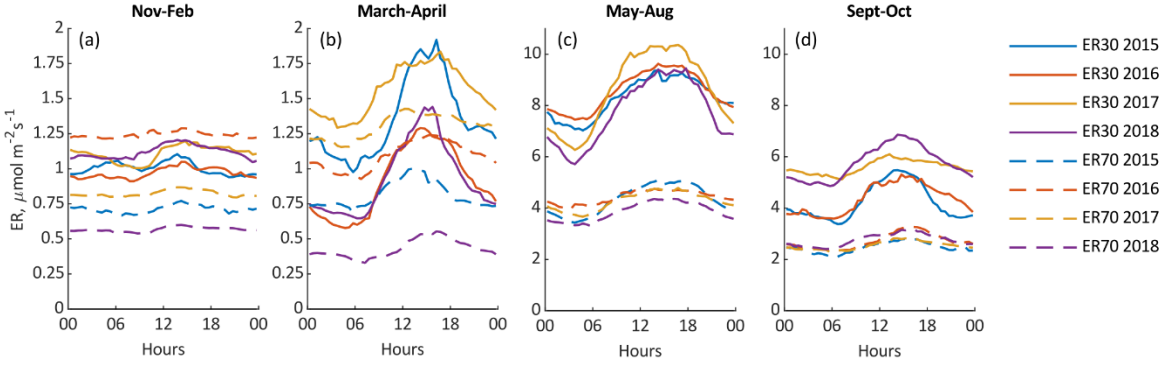

https://doi.org/10.5194/egusphere-2022-384
Preprint. Discussion started: 9 June 2022
© Author(s) 2022. CC BY 4.0 License.

Fig. 8. Median diurnal cycle of ecosystem respiration calculated by daytime data-based method. Solid lines are ER30 and dashed lines are ER70.

3.4 Seasonal cycle

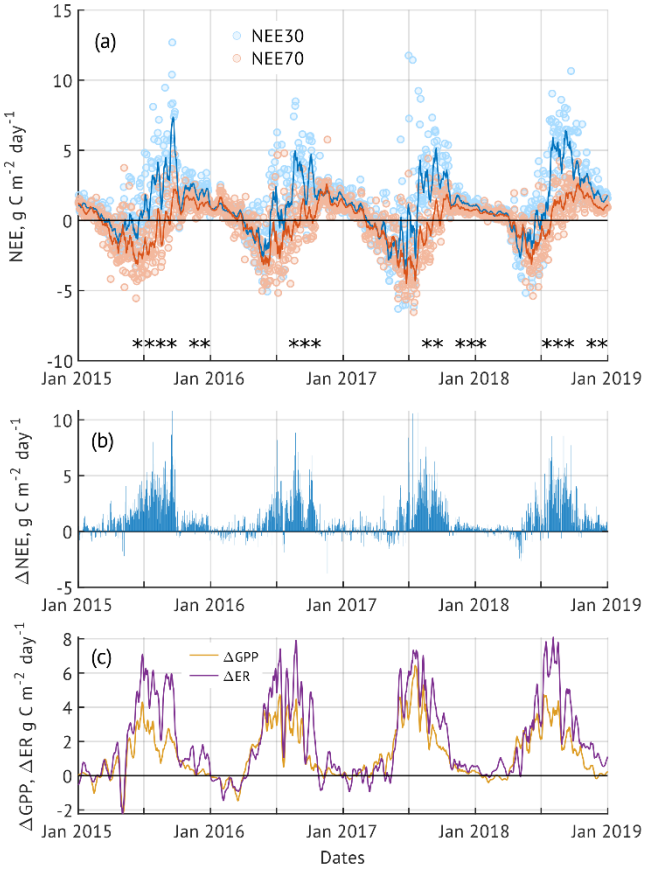

Fig. 9. Seasonal dynamics of the net ecosystem exchange (a, the circles represent daily sums, and the lines are 10 days running averages. Asterisks mark the months with significant differences); the daily difference between NEE30 and NEE70 (ΔNEE = NEE30-NEE70, b) and the difference between GPP and ER (c, 10-days running averages) calculated from the 2 systems data (ΔGPP = GPP30-GPP70; ΔER = ER30-ER70).

NEE measured by both systems demonstrated a distinctive seasonal pattern, with an ecosystem being the source of CO_2 during the dormancy periods (Fig. 9a). The switch from the net carbon source status to the net carbon sink happened at approximately the same time for both systems in March. During the winter and until the second part of March, NEE30 and NEE70 were similar; ΔNEE had small positive and negative values (Fig. 9b). Starting from the second part of March and until the second part of July, NEE30 was more positive than NEE70 except for some separate days. However, no significant difference was found for either of the months. From the second part of July until the middle of September, NEE30 was consistently higher in all the days and on average above zero (carbon source). Some days in the beginning of autumn

https://doi.org/10.5194/egusphere-2022-384
Preprint. Discussion started: 9 June 2022
© Author(s) 2022. CC BY 4.0 License.

exhibited lower NEE30, while after the first half of November, it was higher almost consistently until the end of the calendar year. The difference between the daily fluxes of the two systems was significant only in separate summer and autumn months: July-September and November-December in 2015, August-October in 2016, August-September and November-January in 2017, July-September and November-December in 2018 (Table A1).

While both GPP30 and ER30 were higher than GPP70 and ER70, respectively, during the vegetation periods of all the years (Fig. 9c), the difference in ER was higher, thus explaining why NEE30 was more positive than NEE70 (Fig. 9a-b). Yearly average ΔGPP varied between 0.93 ± 1.38 g C m^{-2} day^{-1} in 2015 and 1.57 ± 1.89 g C m^{-2} day^{-1} in 2017. The minimum ΔER was in 2016 (1.83 ± 2.75 g C m^{-2} day^{-1}) and the maximum in 2018 (2.30 ± 2.49 g C m^{-2} day^{-1})

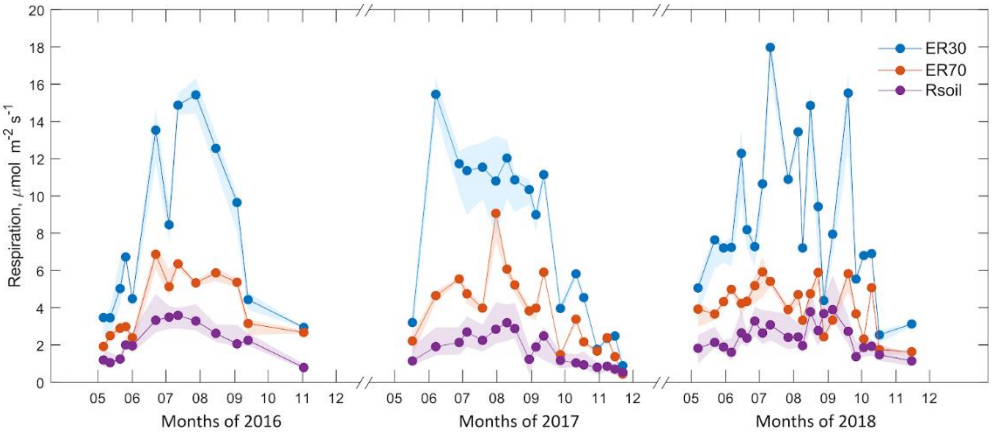

Fig. 10. Seasonal dynamics of ecosystem (ER30 and ER70) and forest floor (Rs) respiration. Ecosystem respiration is represented by daily medians of daytime fluxes for the dates corresponding to manual soil respiration measurements. Forest floor respiration is daily medians of all the measurements done within the given day (3 sample plots pooled together). Shaded areas represent upper and lower quartiles.

The seasonal dynamics of forest floor respiration (Rs) was similar to both systems' daytime ER modelled for the same day (Fig. 10), although ER70 followed the pattern more closely. On average daily medians of ER30 and ER70 were higher than Rs for 6.11±3.71 and 1.88±1.26 μmol m^{-2} s^{-1} respectively. Rs share was 0.30 and 0.57 of ER30 and ER70, respectively.

3.5 The differences by wind direction

The highest difference between the two systems was observed in the darker periods (Rg<130 W m^{-2}) of May-October of all the studied years (Fig. 7c). As both footprints are highly heterogeneous, we tested if this difference was similar over different wind directions. Wind sectors 100° - 130° and 200° - 240° demonstrated much higher ΔNEE than all other wind directions (Fig. 11a). The same wind sectors contain tower guy wires (solid black lines in Fig. 11). While this heterogeneity could result from a temperature and radiation difference between the periods dominated by a certain wind direction, that is not the case as air temperature and radiation for the same periods were relatively equally distributed (Fig. 11b & c).

https://doi.org/10.5194/egusphere-2022-384
Preprint. Discussion started: 9 June 2022
© Author(s) 2022. CC BY 4.0 License.

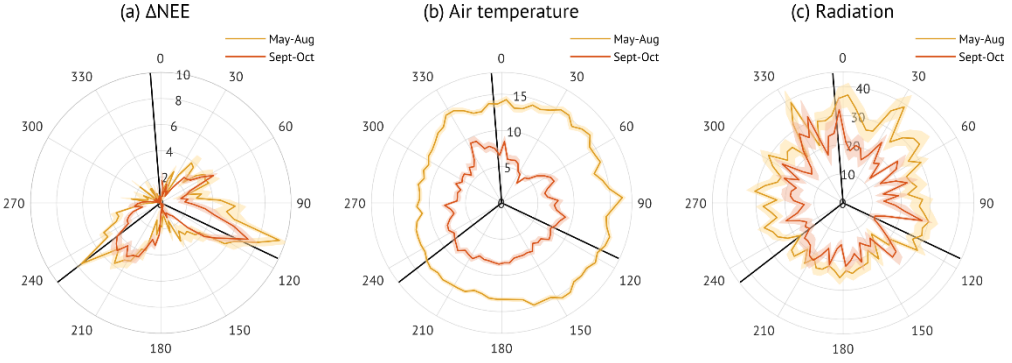

305

Fig. 11. ΔNEE (a, NEE30 - NEE70, µmol m^{-2} s^{-1}), air temperature (b, °C) and global radiation (c, W m^{-2}) of different wind directions (degrees from North), averages of 5° bins. The data from 2015-2018 and solar radiation lower than 130 W m^{-2}. Black lines denote tower guy wires tunnels position. The two periods marked by different colours and shaded areas represent standard errors.

https://doi.org/10.5194/egusphere-2022-384
Preprint. Discussion started: 9 June 2022
© Author(s) 2022. CC BY 4.0 License.

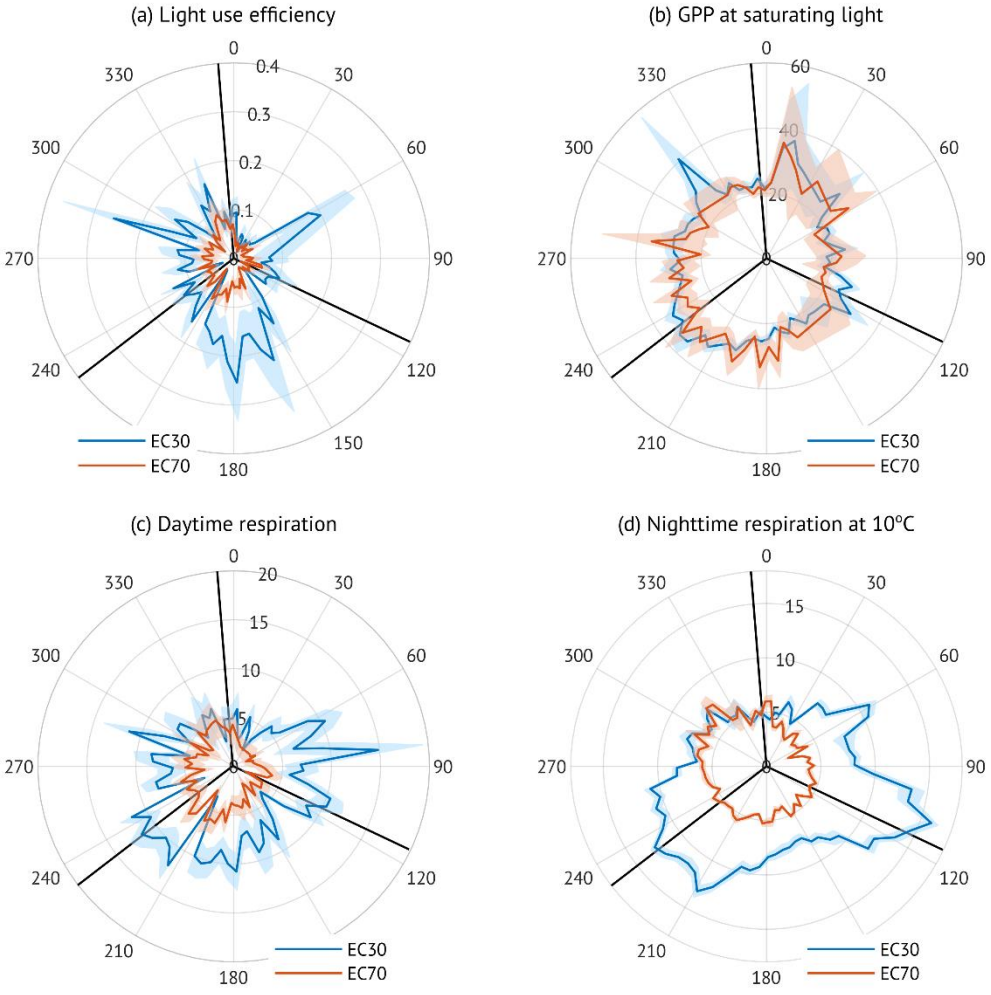

310

Fig. 12. Parameters of Michaelis-Menten (a-c) and Lloyd & Taylor (d) equations obtained from the fitting to 5-degree of wind direction bins of measured NEE (NEE_{day} vs Rg for Michaelis-Menten and NEE_{night} vs T_{air} for Lloyd & Taylor) in May-October of 2015-2018. Only statistically significant ($p<0.05$) values. Shaded areas represent standard errors. Black lines denote tower guy wire tunnels.

315 A similar pattern was observed for the parameters of Michaelis-Menten and Lloyd & Taylor models (Fig. 12). Light use efficiency (Fig. 12a) was similar for the two systems in the 345° - 28° wind sector, while for all the others, EC30 had higher values. GPP at saturating light (Fig. 12b) had mostly similar values between the two systems across all the wind directions. Nighttime ER at 10 °C (Fig. 12d) had a pattern that was similar to the differences in ΔNEE (Fig. 11a), further confirming that it was not caused by the temperature differences. The 294°-9° wind sector demonstrated similar values for both systems. Due
320 to the better mixing, daytime respiration (Fig. 12c) was more evenly distributed over the wind directions, with ER30 being constantly higher than ER70.

https://doi.org/10.5194/egusphere-2022-384
Preprint. Discussion started: 9 June 2022
© Author(s) 2022. CC BY 4.0 License.

3.6 Directional heterogeneity correction

Directional heterogeneity correction resulted in the decrease of cumulative NEE30 values for 229 g C m^{-2} over the four years. The effect was similar for NEE70 with the shift of 115 g C m^{-2} towards more negative values. The correction has neither affected the shape of the seasonal cycle nor the differences between the systems (Figure A1. Monthly sums (A) and cumulative NEE (B) before (solid lines) and after (dashed lines) the directional heterogeneity correction (Hadden and Grelle, 2017).Fig. A1). For most of the months for both systems, directional heterogeneity correction resulted in the shift of NEE towards more negative values. The average difference was 9.13 ± 7.89 and 4.77 ± 3.25 g C m^{-2} $month^{-1}$ for NEE30 and NEE70, respectively. The differences were significant ($p<0.0001$) for both systems before and after the gap-filling. The results of the correction sensitivity analysis can be found in Fig. A3 and Table A2. No significant difference between the NEE corrected using different wind sector sizes was found neither before nor after the gap-filling ($p=0.9$). The majority of correction multipliers were smaller than 1 for all the six wind direction sector sizes and both systems (Fig. A2), indicating that the correction reduced the flux values in all the cases. As a result, annual NEE shifted towards more negative values (weaker source or stronger sink) for all the years/wind sector size choices with single exceptions. The wind sector size had a significant influence only in 2018 when the annual sums were decreasing with the increase in wind sector size for both systems (EC30: slope = -0.54356; R^2=0.821; p=0.00812; EC70: slope= -0.64817; R^2=0.789; p= 0.0113).

3.7 Annual budgets

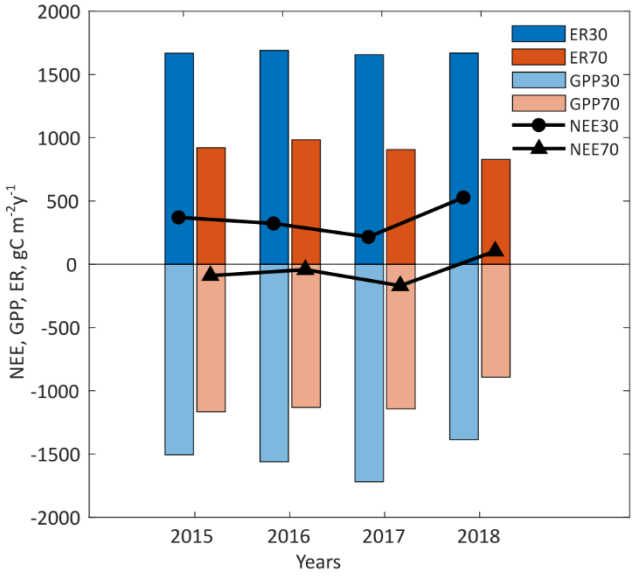

Fig. 13. Yearly sums of net ecosystem exchange (NEE), gross primary production (GPP) and ecosystem respiration (ER) from two eddy-covariance systems (EC30 and EC70). NEE was corrected for directional heterogeneity and gap-filled using the MDS technique. ER and GPP were calculated using the daytime flux partitioning approach and measured NEE values that were not corrected for directional heterogeneity.

https://doi.org/10.5194/egusphere-2022-384
Preprint. Discussion started: 9 June 2022
© Author(s) 2022. CC BY 4.0 License.

During the four studied years, the ecosystem within the EC30 footprint area was a net source of CO_2 with an average of 359±65 g C m^{-2} y^{-1} (Fig. 13). The ecosystem respiration was very stable (1659±6 g C m^{-2} y^{-1}, mean±SE). The differences in NEE were caused by the changes in GPP (-1542±69 g C m^{-2} y^{-1}). The lowest net carbon release occurred in 2017 (216 g C m^{-2} y^{-1}) due to the highest GPP (-1719 g C m^{-2} y^{-1}) over the study period. The reduction of GPP in the hot summer of 2018 (-1387 g C m^{-2} y^{-1}) led to the highest NEE (528 g C m^{-2} y^{-1}).

The ecosystem in the footprint area of EC70 changed from being a weak net carbon sink in 2015 and 2016 to a moderate net sink in 2017 and a net source in 2018 with an average of -50±58 g C m^{-2} y^{-1} over the four years (Fig. 13). ER was 910±32 g C m^{-2} y^{-1}, and GPP was -1084±84 g C m^{-2} y^{-1}. Out of the four years, the highest carbon sequestration occurred in 2017 (-170 g C m^{-2} y^{-1}) due to the lowest ER (907 g C m^{-2} y^{-1}). In 2018 NEE70 was positive (104 g C m^{-2} y^{-1}), and both GPP and ER had the smallest values over the studied period (-892 and 828 g C m^{-2} y^{-1}, respectively).

4. Discussion

4.1 Sensors location

Eddy-covariance (EC) method relies on the assumption that the study area is flat and homogeneous (Baldocchi, 2008). The latter is rarely found in managed forest ecosystems (Chen et al., 2012; Sogachev et al., 2004). One strategy in EC system placement is to maximise the spatial representativeness of the ecosystem of interest in the flux tower footprint area (Chen et al., 2012; Munger et al., 2012). Measurement height is an essential factor in achieving this representativeness. Ideally, the measurement system is located in the inertial sublayer of the atmospheric boundary layer, where the fluxes are assumed constant with height. At the same time, the ecosystem of interest should cover the majority of the footprint area. Having placed two EC systems on the tower at 30 m and 70 m height, we covered both criteria. The upper system EC70 is located in the inertial sublayer but contains a wider variety within the footprint (Fig. 4) and can be categorised as a landscape tower system (Chi et al., 2019; Haszpra et al., 2005). The lower system EC30 is located within the roughness sublayer, where the canopy structure, disturbances, and eventual source-sink differences play a more prominent role. On the other hand, the EC30 footprint is more homogeneous and has a clearly defined structure of clear-cuts and forested areas.

4.2 Differences in diurnal and seasonal cycles

The fluxes measured with both systems changed within a similar range on a half-hourly scale, with noticeable high peaks from EC30 happening at low light conditions (Fig. 5). Nevertheless, the shapes of the median diurnal cycles (Fig. 6) were similar for both heights, with maximum uptake around noon, as was already observed for other similar ecosystems (Chi et al., 2019; Noe et al., 2011). The differences between the median diurnal cycles were most prominent during the vegetation period and the autumn months consistently for all studied years. Over the year, the difference between the two systems remained small but significant in the dormancy period and was absent in spring (Fig. 9, Table A1). The most pronounced

https://doi.org/10.5194/egusphere-2022-384
Preprint. Discussion started: 9 June 2022
© Author(s) 2022. CC BY 4.0 License.

difference was observed during May to August and autumn months (September – October), with EC30 demonstrating more positive fluxes than EC70. ΔNEE was the highest at u* 0.4 m s^{-1} and decreased with the further increase of friction velocity. At the time of the study and manuscript preparation, we found no published data on eddy-covariance CO_2 fluxes measured from the same tower at two different heights above the canopy. However, Cho et al. (2013) reported a height-dependent difference in water vapour flux when comparing data from 30 and 100 m EC systems mounted on a tall tower located in a mixed vegetation cover (70% forests, 30% agricultural fields) in north-western Thailand. Lindroth et al. (2010) found a sensible heat flux divergence between the 35 and 70m height measurements but no difference in latent heat flux over a mature coniferous forest in central Sweden.

4.3 Differences in the annual balance and comparison to other similar ecosystems

According to the annual balance, the ecosystem under the EC30 was a strong net source of CO_2 during all four studied years, while EC70 was switching between a weak net sink and a weak source (Fig. 13, Table 2). The Liispõllu site (SMEAR Estonia substation) that was the focus of our previous studies (Krasnova et al., 2019; Noe et al., 2011) is a birch and spruce mixed forest located within the EC70 footprint area. In the year 2015, it was a strong net sink of CO_2. In the same year, GPP70 was slightly smaller (-1166 gC m^{-2} y^{-1}) while ER70 was much higher (921 gC m^{-2} y^{-1}). The carbon balance of a six-year-old Scots pine stand located 8 km from SMEAR Estonia was analysed by Uri et al. (2019). While this particular study site was not within reach of EC70, similar young forest stands can also be found closer to the tower. Both NEE30 and NEE70 in the corresponding year (2016) were positive, with values higher and lower than the young pine stand (371 and 4 gC m^{-2} y^{-1} respectively). Both GPP30 and ER30 for that year were much higher (-1557 and 1653 gC m^{-2} y^{-1} respectively), while the GPP70 was closer to the young pine stand (-1131 gC m^{-2} y^{-1}) and ER70 was smaller (984 gC m^{-2} y^{-1})

Table 2. The annual budgets of the ecosystem under study and other similar ones. The NEE values in brackets are calculated after the directional heterogeneity correction with 45o wind sectors size.

Site	Measurement height, m	Year(s)	NEE, g C m^{-2} y^{-1}	GPP, g C m^{-2} y^{-1}	ER, g C m^{-2} y^{-1}	Reference
SMEAR Estonia atmospheric tower: Scots pine, Norway spruce, Birch sp. 58°16'N	30	2015 – 2018	416 ± 124 (359 ± 130)*	-1542 ± 138	1659 ± 11	This study
	70		-21 ± 120 (-46 ± 120)*	-1083 ±128	910 ± 64	
SMEAR Estonia Liispõllu site:	24	2015	−586 ± 45	-1243	626	(Krasnova et al., 2019)

https://doi.org/10.5194/egusphere-2022-384
Preprint. Discussion started: 9 June 2022
© Author(s) 2022. CC BY 4.0 License.

Norway spruce and Birch sp. 58°16'N						
Young (6 y.o) Scots pine forest, Estonia 58°17′N	4.35	2016	119 ± 36	-987	1106	(Uri et al., 2019)
Norunda: Scots pine, Norway spruce Sweden 60°05′N	33.5	2007 – 2008	412	-1658	2070	(Lindroth et al., 2018)
		2015 – 2018	364 ± 73	-1330 ± 108	1576 ± 122	(Mölder et al., 2020)
Norway spruce plantation in Denmark 56.07°N	38	2009 – 2014	−691 ± 143	−1744 ± 132	1053 ± 50	(Jensen et al., 2017)
Hyytiälä: Scots pine forest 61°50′N	33	2015 – 2018	-284 ± 28	-1167 ± 41	941 ± 71	(Mammarella and ICOS Ecosystem Thematic Centre, 2020)
Boreal landscape in Sweden 64°15′N	70	03/2016 - 02/2017	-132 ± 8	-824 ± 18	692 ± 21	(Chi et al., 2019)
		03/2017 - 02/2018	−57 ± 9	−785 ± 20	728 ± 23	
Mixed vegetation landscape in Hungary 46°57′N	82	1997 – 2004	-35 ± 59	-1096 ± 180	1074 ± 109	(Haszpra et al., 2005)

Several long-term studies of CO_2 flux from similar forests in Sweden also reported annual net source values. A Norway spruce forest in northern Sweden (64°07′N) had a positive annual sum of NEE in 2010-2013 with a range similar to NEE30 of our study (Hadden and Grelle, 2016). In another research by the same authors (Hadden and Grelle, 2017), the unmanaged primary boreo-nemoral forest dominated by Scots pine and Norway spruce (59°54′N) was a net source of CO_2 with the release of 25 mg CO_2 ha^{-1} (68.2 g C m^{-2}) per 10 years (2004-2014). Another hemiboreal mixed forest of Scots pine and Norway spruce in central Sweden (ICOS station Norunda, 60°05′N) was also a net source of CO_2 during all the 10 years of measurements (2007-2016) (Lindroth et al., 2018). The average NEE of the two years before the thinning is similar to NEE30 in the current study. ER of the Norunda forest was higher, while GPP was in the same range. The average values for

https://doi.org/10.5194/egusphere-2022-384
Preprint. Discussion started: 9 June 2022
© Author(s) 2022. CC BY 4.0 License.

the same years as in the current study are slightly lower (Mölder et al., 2020) but fit within the standard deviation range of our reported values.

However, Jensen et al. (2017) reported high yearly sequestration for the Norway spruce plantation in Denmark (56.07°N) with an average of -691 ± 143 g C m^{-2} y^{-1} over the six years (2009-2014). The average GPP was similar to the current study (-1744 ± 132 g C m^{-2} y^{-1}), the difference comes from ER that was much lower (1053 ± 50 g C m^{-2} y^{-1}). A Scots pine forest in Finland (ICOS station Hyytiälä, 61°50′N) was a net sink during all years of a long-term measurement period of 1996-2018 (Mammarella and ICOS Ecosystem Thematic Centre, 2020). Over the same years as the current study, the average NEE was -284 ± 28 g C m^{-2} y^{-1}. For the same period, the average GPP was 1167 ± 41 gC m^{-2} y^{-1} and ER was 941 ± 71 g C m^{-2} y^{-1} that is much closer to the values obtained from the EC70, than EC30 in our study.

Chi et al. (2019) estimated the carbon fluxes from the height of 70 m over a managed boreal landscape in northern Sweden (64°15′N). They reported a stronger net sink of -87 ± 6 g C m^{-2} yr^{-1} (the average of March 1, 2016, to February 28, 2018), with forests being the origin of 87% of flux measurements. Haszpra et al. (2005) analysed fluxes measured from an 82 m height over a landscape in Hungary with only 30% of forest and woodland (60% arable land and 10% other types). They also noted that NEE estimated from the tall tower could be shifted toward more positive values due to the anthropogenic activity in such a large footprint area.

4.4 The influence of clear-cut areas

The observed difference between the two heights nighttime fluxes of the second part of the year was irregularly distributed over the wind direction sectors, pointing to the potential existence of CO_2 hotspots that were “captured” by EC30 but “mixed away” by the height of EC70 (Fig. 11, 12). While the distribution of air temperature over the wind direction sectors for the same periods did not match that of the NEE difference (Fig. 11), the overall difference during low light periods in May-August was increasing with the rise of air temperature. Rebmann et al. (2010) also reported high positive nighttime carbon fluxes coming from a certain wind direction in a complex forest site in Germany. The increased respiration values were observed at u*>0.4 m s^{-1}. The authors suggest that the drainage was causing the upwind transport of enriched air from the valley. Similarly, Cook et al. (2004) observed high ER values in an upland deciduous forest in the US. The “venting anomalies” were observed for nighttime and early morning fluxes coming from certain wind directions. The possible causes included cold-air drainage into low-lying areas or local respiration “hot spots”. The latter was further confirmed by the increase of anomaly magnitude with rising soil temperature and the decrease of magnitude when soil moisture exceeded 0.35 m^3 m^{-3}.

The EC30 footprint features higher proportions of deforested areas (clear-cuts), thus making it a potentially weaker net carbon sink or a stronger net carbon source. The difference in ecosystem respiration was found for both, nighttime and daytime values (Fig. 8), with similar seasonality as observed for ΔNEE (Fig. 9b). The possible clear-cuts’ influence on our measurements is further confirmed by the NEE30 seasonal dynamics (Fig. 9a) being much closer by its shape to the seasonal dynamics of clear-cut areas NEE (Grant et al., 2010; Mamkin et al., 2019; Uri et al., 2019) than that of forests (Chi et al.,

https://doi.org/10.5194/egusphere-2022-384
Preprint. Discussion started: 9 June 2022
© Author(s) 2022. CC BY 4.0 License.

2019; Jensen et al., 2017; Krasnova et al., 2019). Moreover, the yearly cycle of forest floor respiration measured in the forest stands around the tower featured less similarities to ER30, compared to ER70 (Fig. 10). Nevertheless, the average Rs/ER for our measurement period was 0.30 for ER30 and 0.57 for ER70, which falls within the 0.3-0.8 range previously reported for various ecosystems (Barba et al., 2018; Davidson and Janssens, 2006).

The observed wind field irregularities (Fig. 3,4) could contribute to differences between the fluxes measured from the two heights. If the overrepresentation of wind directions coming from the CO_2 hotspots was one of the reasons, directional heterogeneity correction would diminish them. However, while shifting both NEE30 and NEE70 towards more negative values, the correction altered neither the difference between them nor the specific clearcut-like shape of the NEE30 seasonal cycle (Fig. A1). Clear-cuts act as net carbon sources for years after the disturbance due to the direct removal of vegetation, soil disturbance and the increase in heterotrophic respiration (Grant et al., 2010; Kolari et al., 2004; Noormets et al., 2015, 2012). In the low mixing conditions typical for the night-time periods, the carbon-enriched air may accumulate under the measurement point. The following increase in wind speed and friction velocity would cause the transport of this air through the open guy wire tunnels, subsequently resulting in high flux values. Such values would not be eliminated during the filtering, as the mixing during the corresponding half-hours is sufficient.

5. Conclusions

In a comparison of the CO_2 fluxes measured with eddy-covariance systems mounted at two different heights we demonstrate the importance of landscape heterogeneity in the carbon flux budgets. In case of SMEAR Estonia, carbon-enriched air originated from clear-cut areas was not fully mixed and transported up in the following hours predominantly through the guy wire tunnels. These local heterogeneities were detected by the system located 10 m above the canopy and strongly affected the yearly accumulated budget. More detailed research of possible decoupling as well as soil respiration measurements at clear-cuts within the tower footprint are needed to confirm this conclusion.

The higher located system (more than 3 times the canopy height) demonstrated a more balanced yearly budget with the numbers closer to the expected values for the forested ecosystem. Due to better mixing and natural integration, it was oblivious to the local disturbances in the footprint, thus confirming our hypothesis.

Our work confirms that long-term ecosystem-scale measurements need to consider the footprint heterogeneity (Aubinet et al., 2002; Finnigan, 2004; Vesala et al., 2008, 2004). In addition to the variability in forest age, hight and tree species composition, station installation and ongoing wood harvesting introduce additional disturbance to the forest integrity. A sensor placement height in a managed heterogeneous forest ecosystem must be chosen in accordance with the features of the landscape and the aim of the study. The eddy-covariance system located at the lowest possible distance from the canopy detects the footprint irregularities and allows to assess their influence on the CO_2 fluxes. In order to obtain a more integrated carbon signal of the heterogeneous forest stand, we recommend to place the eddy-covariance system at a higher point to allow for natural mixing and less biased annual estimates.

https://doi.org/10.5194/egusphere-2022-384
Preprint. Discussion started: 9 June 2022
© Author(s) 2022. CC BY 4.0 License.

Data availability. The data can be requested from the corresponding author.

Authors contributions. AK developed the concept of the paper, performed the eddy-covariance flux computations, statistical analysis, and wrote the paper with contributions of other co-authors. DK designed and performed forest floor respiration measurements and data analysis and wrote corresponding texts. HPEC curated the data acquisition. SMN processed wind profile data and participated in the conception and writing of the paper. All co-authors reviewed the paper.

Competing interests. The authors declare that they have no conflict of interest

Acknowledgements. This study was financially supported by the European Union's Horizon 2020 research and innovation programme under Grant agreement No. 689443 via project iCUPE (Integrative and Comprehensive Understanding on Polar Environments, ERA-PLANET), the Estonian Ministry of Sciences, Estonia projects (Grant Nos. P180021, P180274, P200196), the Estonian Research Infrastructures Roadmap project Estonian Environmental Observatory (3.2.0304.11-0395), the Estonian Environmental Investment Centre (KIK, grant no. 3-2.8/6574), the Estonian Research Council (project PRG1674).

References

Ahti, T., Hämet-Ahti, L., and Jalas, J.: Vegetation zones and their sections in northwestern Europe, 5, 169–211, 1968.

Aubinet, M., Heinesch, B., and Longdoz, B.: Estimation of the carbon sequestration by a heterogeneous forest: night flux corrections, heterogeneity of the site and inter-annual variability, 8, 1053–1071, https://doi.org/10.1046/j.1365-2486.2002.00529.x, 2002.

Baldocchi, D.: Measuring fluxes of trace gases and energy between ecosystems and the atmosphere - the state and future of the eddy covariance method, Glob Change Biol, 20, 3600–3609, https://doi.org/10.1111/gcb.12649, 2014.

Barba, J., Cueva, A., Bahn, M., Barron-Gafford, G. A., Bond-Lamberty, B., Hanson, P. J., Jaimes, A., Kulmala, L., Pumpanen, J., Scott, R. L., Wohlfahrt, G., and Vargas, R.: Comparing ecosystem and soil respiration: Review and key challenges of tower-based and soil measurements, Agricultural and Forest Meteorology, 249, 434–443, https://doi.org/10.1016/j.agrformet.2017.10.028, 2018.

Barcza, Z., Kern, A., Davis, K. J., and Haszpra, L.: Analysis of the 21-years long carbon dioxide flux dataset from a Central European tall tower site, Agricultural and Forest Meteorology, 290, 108027, https://doi.org/10.1016/j.agrformet.2020.108027, 2020.

Burba, G.: Eddy covariance method for scientific, industrial, agricultural, and regulatory applications: a field book on measuring ecosystem gas exchange and areal emission rates, LI-COR Biosciences, Lincoln, Nebraska, 331 pp., 2013.

Chi, J., Nilsson, M. B., Kljun, N., Wallerman, J., Fransson, J. E. S., Laudon, H., Lundmark, T., and Peichl, M.: The carbon balance of a managed boreal landscape measured from a tall tower in northern Sweden, Agricultural and Forest Meteorology, 274, 29–41, https://doi.org/10.1016/j.agrformet.2019.04.010, 2019.

https://doi.org/10.5194/egusphere-2022-384
Preprint. Discussion started: 9 June 2022
© Author(s) 2022. CC BY 4.0 License.

Chi, J., Nilsson, M. B., Laudon, H., Lindroth, A., Wallerman, J., Fransson, J. E. S., Kljun, N., Lundmark, T., Ottosson Löfvenius, M., and Peichl, M.: The Net Landscape Carbon Balance—Integrating terrestrial and aquatic carbon fluxes in a managed boreal forest landscape in Sweden, Glob Change Biol, 26, 2353–2367, https://doi.org/10.1111/gcb.14983, 2020.

Cho, J., Kim, W., Miyazaki, S., Komori, D., Kim, H., Han, K.-S., Kanae, S., and Oki, T.: Difference in the Priestley–Taylor coefficients at two different heights of a tall micrometeorological tower, Agricultural and Forest Meteorology, 180, 97–101, https://doi.org/10.1016/j.agrformet.2013.05.007, 2013.

Cook, B. D., Davis, K. J., Wang, W., Desai, A., Berger, B. W., Teclaw, R. M., Martin, J. G., Bolstad, P. V., Bakwin, P. S., Yi, C., and Heilman, W.: Carbon exchange and venting anomalies in an upland deciduous forest in northern Wisconsin, USA, Agricultural and Forest Meteorology, 126, 271–295, https://doi.org/10.1016/j.agrformet.2004.06.008, 2004.

Davidson, E. A. and Janssens, I. A.: Temperature sensitivity of soil carbon decomposition and feedbacks to climate change, Nature, 440, 165–173, https://doi.org/10.1038/nature04514, 2006.

European research agency: European Forest Types. Categories and types for sustainable forest management reporting and policy, 2016.

Ezhova, E., Ylivinkka, I., Kuusk, J., Komsaare, K., Vana, M., Krasnova, A., Noe, S., Arshinov, M., Belan, B., Park, S.-B., Lavrič, J. V., Heimann, M., Petäjä, T., Vesala, T., Mammarella, I., Kolari, P., Bäck, J., Rannik, Ü., Kerminen, V.-M., and Kulmala, M.: Direct effect of aerosols on solar radiation and gross primary production in boreal and hemiboreal forests, Atmos. Chem. Phys., 18, 17863–17881, https://doi.org/10.5194/acp-18-17863-2018, 2018.

Fernández-Martínez, M., Vicca, S., Janssens, I. A., Ciais, P., Obersteiner, M., Bartrons, M., Sardans, J., Verger, A., Canadell, J. G., Chevallier, F., Wang, X., Bernhofer, C., Curtis, P. S., Gianelle, D., Grünwald, T., Heinesch, B., Ibrom, A., Knohl, A., Laurila, T., Law, B. E., Limousin, J. M., Longdoz, B., Loustau, D., Mammarella, I., Matteucci, G., Monson, R. K., Montagnani, L., Moors, E. J., Munger, J. W., Papale, D., Piao, S. L., and Peñuelas, J.: Atmospheric deposition, CO2, and change in the land carbon sink, Sci Rep, 7, 9632, https://doi.org/10.1038/s41598-017-08755-8, 2017.

Finnigan, J.: The footprint concept in complex terrain, Agricultural and Forest Meteorology, 127, 117–129, https://doi.org/10.1016/j.agrformet.2004.07.008, 2004.

Friedlingstein, P., Jones, M. W., O'Sullivan, M., Andrew, R. M., Hauck, J., Peters, G. P., Peters, W., Pongratz, J., Sitch, S., Le Quéré, C., Bakker, D. C. E., Canadell, J. G., Ciais, P., Jackson, R. B., Anthoni, P., Barbero, L., Bastos, A., Bastrikov, V., Becker, M., Bopp, L., Buitenhuis, E., Chandra, N., Chevallier, F., Chini, L. P., Currie, K. I., Feely, R. A., Gehlen, M., Gilfillan, D., Gkritzalis, T., Goll, D. S., Gruber, N., Gutekunst, S., Harris, I., Haverd, V., Houghton, R. A., Hurtt, G., Ilyina, T., Jain, A. K., Joetzjer, E., Kaplan, J. O., Kato, E., Klein Goldewijk, K., Korsbakken, J. I., Landschützer, P., Lauvset, S. K., Lefèvre, N., Lenton, A., Lienert, S., Lombardozzi, D., Marland, G., McGuire, P. C., Melton, J. R., Metzl, N., Munro, D. R., Nabel, J. E. M. S., Nakaoka, S.-I., Neill, C., Omar, A. M., Ono, T., Peregon, A., Pierrot, D., Poulter, B., Rehder, G., Resplandy, L., Robertson, E., Rödenbeck, C., Séférian, R., Schwinger, J., Smith, N., Tans, P. P., Tian, H., Tilbrook, B., Tubiello, F. N., van der Werf, G. R., Wiltshire, A. J., and Zaehle, S.: Global Carbon Budget 2019, Earth Syst. Sci. Data, 11, 1783–1838, https://doi.org/10.5194/essd-11-1783-2019, 2019.

https://doi.org/10.5194/egusphere-2022-384
Preprint. Discussion started: 9 June 2022
© Author(s) 2022. CC BY 4.0 License.

Grant, R. F., Barr, A. G., Black, T. A., Margolis, H. A., Mccaughey, J. H., and Trofymow, J. A.: Net ecosystem productivity of temperate and boreal forests after clearcutting—a Fluxnet-Canada measurement and modelling synthesis, Tellus B: Chemical and Physical Meteorology, 62, 475–496, https://doi.org/10.1111/j.1600-0889.2010.00500.x, 2010.

Hadden, D. and Grelle, A.: Net CO2 emissions from a primary boreo-nemoral forest over a 10 year period, Forest Ecology and Management, 398, 164–173, https://doi.org/10.1016/j.foreco.2017.05.008, 2017.

Haszpra, L., Barcza, Z., Davis, K. J., and Tarczay, K.: Long-term tall tower carbon dioxide flux monitoring over an area of mixed vegetation, Agricultural and Forest Meteorology, 132, 58–77, https://doi.org/10.1016/j.agrformet.2005.07.002, 2005.

Jensen, R., Herbst, M., and Friborg, T.: Direct and indirect controls of the interannual variability in atmospheric CO2 exchange of three contrasting ecosystems in Denmark, Agricultural and Forest Meteorology, 233, 12–31, https://doi.org/10.1016/j.agrformet.2016.10.023, 2017.

Keenan, T. F. and Williams, C. A.: The Terrestrial Carbon Sink, Annu. Rev. Environ. Resour., 43, 219–243, https://doi.org/10.1146/annurev-environ-102017-030204, 2018.

Kolari, P., Pumpanen, J., Rannik, Ü., Ilvesniemi, H., Hari, P., and Berninger, F.: Carbon balance of different aged Scots pine forests in Southern Finland, 10, 1106–1119, https://doi.org/10.1111/j.1529-8817.2003.00797.x, 2004.

Krasnova, A., Kukumägi, M., Mander, Ü., Torga, R., Krasnov, D., Noe, S. M., Ostonen, I., Püttsepp, Ü., Killian, H., Uri, V., Lõhmus, K., Sõber, J., and Soosaar, K.: Carbon exchange in a hemiboreal mixed forest in relation to tree species composition, Agricultural and Forest Meteorology, 275, 11–23, https://doi.org/10.1016/j.agrformet.2019.05.007, 2019.

Kulmala, M., Nieminen, T., Nikandrova, A., Lehtipalo, K., Manninen, H. E., Kajos, M. K., Kolari, P., Lauri, A., Petäjä, T., Krejci, R., Hansson, H.-C., Swietlicki, E., Lindroth, A., Christensen, T. R., Arneth, A., Hari, P., Bäck, J., Vesala, T., and Kerminen, V.-M.: CO2-induced terrestrial climate feedback mechanism: From carbon sink to aerosol source and back, 19, 122–131, 2014.

Lappalainen, H. K., Kerminen, V.-M., Petäjä, T., Kurten, T., Baklanov, A., Shvidenko, A., Bäck, J., Vihma, T., Alekseychik, P., Andreae, M. O., Arnold, S. R., Arshinov, M., Asmi, E., Belan, B., Bobylev, L., Chalov, S., Cheng, Y., Chubarova, N., de Leeuw, G., Ding, A., Dobrolyubov, S., Dubtsov, S., Dyukarev, E., Elansky, N., Eleftheriadis, K., Esau, I., Filatov, N., Flint, M., Fu, C., Glezer, O., Gliko, A., Heimann, M., Holtslag, A. A. M., Hõrrak, U., Janhunen, J., Juhola, S., Järvi, L., Järvinen, H., Kanukhina, A., Konstantinov, P., Kotlyakov, V., Kieloaho, A.-J., Komarov, A. S., Kujansuu, J., Kukkonen, I., Duplissy, E.-M., Laaksonen, A., Laurila, T., Lihavainen, H., Lisitzin, A., Mahura, A., Makshtas, A., Mareev, E., Mazon, S., Matishov, D., Melnikov, V., Mikhailov, E., Moisseev, D., Nigmatulin, R., Noe, S. M., Ojala, A., Pihlatie, M., Popovicheva, O., Pumpanen, J., Regerand, T., Repina, I., Shcherbinin, A., Shevchenko, V., Sipilä, M., Skorokhod, A., Spracklen, D. V., Su, H., Subetto, D. A., Sun, J., Terzhevik, A. Y., Timofeyev, Y., Troitskaya, Y., Tynkkynen, V.-P., Kharuk, V. I., Zaytseva, N., Zhang, J., Viisanen, Y., Vesala, T., Hari, P., Hansson, H. C., Matvienko, G. G., Kasimov, N. S., Guo, H., Bondur, V., Zilitinkevich, S., and Kulmala, M.: Pan-Eurasian Experiment (PEEX): towards a holistic understanding of the feedbacks and interactions in the land–atmosphere–ocean–society continuum in the northern Eurasian region, Atmos. Chem. Phys., 16, 14421–14461, https://doi.org/10.5194/acp-16-14421-2016, 2016.

https://doi.org/10.5194/egusphere-2022-384
Preprint. Discussion started: 9 June 2022
© Author(s) 2022. CC BY 4.0 License.

Lasslop, G., Reichstein, M., Papale, D., Richardson, A. D., Arneth, A., Barr, A., Stoy, P., and Wohlfahrt, G.: Separation of net ecosystem exchange into assimilation and respiration using a light response curve approach: critical issues and global evaluation: SEPARATION OF NEE INTO GPP AND RECO, 16, 187–208, https://doi.org/10.1111/j.1365-2486.2009.02041.x, 2010.

Lindroth, A., Mölder, M., and Lagergren, F.: Heat storage in forest biomass improves energy balance closure, Biogeosciences, 7, 301–313, https://doi.org/10.5194/bg-7-301-2010, 2010.

Lindroth, A., Holst, J., Heliasz, M., Vestin, P., Lagergren, F., Biermann, T., Cai, Z., and Mölder, M.: Effects of low thinning on carbon dioxide fluxes in a mixed hemiboreal forest, Agricultural and Forest Meteorology, 262, 59–70, https://doi.org/10.1016/j.agrformet.2018.06.021, 2018.

Lindroth, A., Holst, J., Linderson, M.-L., Aurela, M., Biermann, T., Heliasz, M., Chi, J., Ibrom, A., Kolari, P., Klemedtsson, L., Krasnova, A., Laurila, T., Lehner, I., Lohila, A., Mammarella, I., Mölder, M., Löfvenius, M. O., Peichl, M., Pilegaard, K., Soosaar, K., Vesala, T., Vestin, P., Weslien, P., and Nilsson, M.: Effects of drought and meteorological forcing on carbon and water fluxes in Nordic forests during the dry summer of 2018, Phil. Trans. R. Soc. B, 375, 20190516, https://doi.org/10.1098/rstb.2019.0516, 2020.

Lloyd, J. and Taylor, J. A.: On the Temperature Dependence of Soil Respiration, Functional Ecology, 8, 315, https://doi.org/10.2307/2389824, 1994.

Mamkin, V., Kurbatova, J., Avilov, V., Ivanov, D., Kuricheva, O., Varlagin, A., Yaseneva, I., and Olchev, A.: Energy and CO2 exchange in an undisturbed spruce forest and clear-cut in the Southern Taiga, Agricultural and Forest Meteorology, 265, 252–268, https://doi.org/10.1016/j.agrformet.2018.11.018, 2019.

Mammarella, I., Peltola, O., Nordbo, A., Järvi, L., and Rannik, Ü.: Quantifying the uncertainty of eddy covariance fluxes due to the use ofdifferent software packages and combinations of processing steps in twocontrasting ecosystems, Atmos. Meas. Tech., 9, 4915–4933, https://doi.org/10.5194/amt-9-4915-2016, 2016.

Moncrieff, J., Clement, R., Finnigan, J., and Meyers, T.: Averaging, Detrending, and Filtering of Eddy Covariance Time Series, in: Handbook of Micrometeorology, vol. 29, edited by: Lee, X., Massman, W., and Law, B., Kluwer Academic Publishers, Dordrecht, 7–31, https://doi.org/10.1007/1-4020-2265-4_2, 2005.

Moncrieff, J. B., Massheder, J. M., de Bruin, H., Elbers, J., Friborg, T., Heusinkveld, B., Kabat, P., Scott, S., Soegaard, H., and Verhoef, A.: A system to measure surface fluxes of momentum, sensible heat, water vapour and carbon dioxide, Journal of Hydrology, 188–189, 589–611, https://doi.org/10.1016/S0022-1694(96)03194-0, 1997.

Munger, J. W., Loescher, H. W., and Luo, H.: Measurement, Tower, and Site Design Considerations, in: Eddy Covariance, edited by: Aubinet, M., Vesala, T., and Papale, D., Springer Netherlands, Dordrecht, 21–58, https://doi.org/10.1007/978-94-007-2351-1_2, 2012.

Noe, S. M., Kimmel, V., Hüve, K., Copolovici, L., Portillo-Estrada, M., Püttsepp, Ü., Jõgiste, K., Niinemets, Ü., Hörtnagl, L., and Wohlfahrt, G.: Ecosystem-scale biosphere–atmosphere interactions of a hemiboreal mixed forest stand at Järvselja, Estonia, Forest Ecology and Management, 262, 71–81, https://doi.org/10.1016/j.foreco.2010.09.013, 2011.

https://doi.org/10.5194/egusphere-2022-384
Preprint. Discussion started: 9 June 2022
© Author(s) 2022. CC BY 4.0 License.

Noe, S. M., Niinemets, Ü., Krasnova, A., Krasnov, D., Motallebi, A., Kängsepp, V., Jõgiste, K., Hõrrak, U., Komsaare, K., Mirme, S., Vana, M., Tammet, H., Bäck, J., Vesala, T., Kulmala, M., Petäjä, T., and Kangur, A.: SMEAR Estonia: Perspectives of a large-scale forest ecosystem – atmosphere research infrastructure, 63, 56–84, https://doi.org/10.1515/fsmu-2015-0009, 2015.

Noormets, A., McNulty, S. G., Domec, J., Gavazzi, M., Sun, G., and King, J. S.: The role of harvest residue in rotation cycle carbon balance in loblolly pine plantations. Respiration partitioning approach, Glob Change Biol, 18, 3186–3201, https://doi.org/10.1111/j.1365-2486.2012.02776.x, 2012.

Noormets, A., Epron, D., Domec, J. C., McNulty, S. G., Fox, T., Sun, G., and King, J. S.: Effects of forest management on productivity and carbon sequestration: A review and hypothesis, Forest Ecology and Management, 355, 124–140, https://doi.org/10.1016/j.foreco.2015.05.019, 2015.

Papale, D., Reichstein, M., Aubinet, M., Canfora, E., Bernhofer, C., Kutsch, W., Longdoz, B., Rambal, S., Valentini, R., Vesala, T., and Yakir, D.: Towards a standardized processing of Net Ecosystem Exchange measured with eddy covariance technique: algorithms and uncertainty estimation, Biogeosciences, 3, 571–583, https://doi.org/10.5194/bg-3-571-2006, 2006.

Rebmann, C., Zeri, M., Lasslop, G., Mund, M., Kolle, O., Schulze, E.-D., and Feigenwinter, C.: Treatment and assessment of the CO2-exchange at a complex forest site in Thuringia, Germany, Agricultural and Forest Meteorology, 150, 684–691, https://doi.org/10.1016/j.agrformet.2009.11.001, 2010.

Rebmann, C., Aubinet, M., Schmid, H., Arriga, N., Aurela, M., Burba, G., Clement, R., De Ligne, A., Fratini, G., Gielen, B., Grace, J., Graf, A., Gross, P., Haapanala, S., Herbst, M., Hörtnagl, L., Ibrom, A., Joly, L., Kljun, N., Kolle, O., Kowalski, A., Lindroth, A., Loustau, D., Mammarella, I., Mauder, M., Merbold, L., Metzger, S., Mölder, M., Montagnani, L., Papale, D., Pavelka, M., Peichl, M., Roland, M., Serrano-Ortiz, P., Siebicke, L., Steinbrecher, R., Tuovinen, J.-P., Vesala, T., Wohlfahrt, G., and Franz, D.: ICOS eddy covariance flux-station site setup: a review, 32, 471–494, https://doi.org/10.1515/intag-2017-0044, 2018.

Reichstein, M., Falge, E., Baldocchi, D., Papale, D., Aubinet, M., Berbigier, P., Bernhofer, C., Buchmann, N., Gilmanov, T., Granier, A., Grunwald, T., Havrankova, K., Ilvesniemi, H., Janous, D., Knohl, A., Laurila, T., Lohila, A., Loustau, D., Matteucci, G., Meyers, T., Miglietta, F., Ourcival, J.-M., Pumpanen, J., Rambal, S., Rotenberg, E., Sanz, M., Tenhunen, J., Seufert, G., Vaccari, F., Vesala, T., Yakir, D., and Valentini, R.: On the separation of net ecosystem exchange into assimilation and ecosystem respiration: review and improved algorithm, Global Change Biol, 11, 1424–1439, https://doi.org/10.1111/j.1365-2486.2005.001002.x, 2005.

Schmid, H. P. and Lloyd, C. R.: Spatial representativeness and the location bias of ¯ux footprints over inhomogeneous areas, 15, 1999.

Soegaard, H.: Carbon dioxide exchange over agricultural landscape using eddy correlation and footprint modelling, Agricultural and Forest Meteorology, 114, 153–173, https://doi.org/10.1016/S0168-1923(02)00177-6, 2003.

https://doi.org/10.5194/egusphere-2022-384
Preprint. Discussion started: 9 June 2022
© Author(s) 2022. CC BY 4.0 License.

Sogachev, A. and Dellwik, E.: Flux footprints for a tall tower in a land–water mosaic area: A case study of the area around the Risø tower, Agricultural and Forest Meteorology, 237–238, 326–339, https://doi.org/10.1016/j.agrformet.2017.02.037, 2017.

Uri, V., Kukumägi, M., Aosaar, J., Varik, M., Becker, H., Aun, K., Krasnova, A., Morozov, G., Ostonen, I., Mander, Ü., Lõhmus, K., Rosenvald, K., Kriiska, K., and Soosaar, K.: The carbon balance of a six-year-old Scots pine (Pinus sylvestris L.) ecosystem estimated by different methods, Forest Ecology and Management, 433, 248–262, https://doi.org/10.1016/j.foreco.2018.11.012, 2019.

Vesala, T., Rannik, Ü., Leclerc, M., Foken, T., and Sabelfeld, K.: Flux and concentration footprints, Agricultural and Forest Meteorology, 127, 111–116, https://doi.org/10.1016/j.agrformet.2004.07.007, 2004.

Vesala, T., Kljun, N., Rannik, Ü., Rinne, J., Sogachev, A., Markkanen, T., Sabelfeld, K., Foken, Th., and Leclerc, M. Y.: Flux and concentration footprint modelling: State of the art, Environmental Pollution, 152, 653–666, https://doi.org/10.1016/j.envpol.2007.06.070, 2008.

Vickers, D. and Mahrt, L.: Quality Control and Flux Sampling Problems for Tower and Aircraft Data, J. Atmos. Oceanic Technol., 14, 512–526, https://doi.org/10.1175/1520-0426(1997)014<0512:QCAFSP>2.0.CO;2, 1997.

Wilczak, J. M., Oncley, S. P., and Stage, S. A.: Sonic Anemometer Tilt Correction Algorithms, Boundary-Layer Meteorology, 99, 127–150, https://doi.org/10.1023/A:1018966204465, 2001.

Wutzler, T., Lucas-Moffat, A., Migliavacca, M., Knauer, J., Sickel, K., Šigut, L., Menzer, O., and Reichstein, M.: Basic and extensible post-processing of eddy covariance flux data with REddyProc, Biogeosciences, 15, 5015–5030, https://doi.org/10.5194/bg-15-5015-2018, 2018.

https://doi.org/10.5194/egusphere-2022-384
Preprint. Discussion started: 9 June 2022
© Author(s) 2022. CC BY 4.0 License.

Appendix

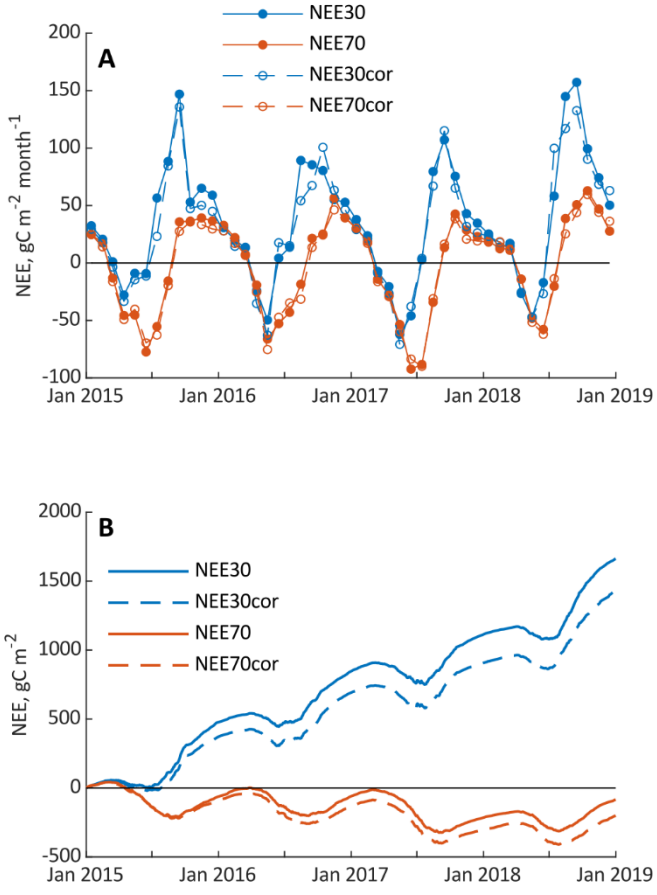

Figure A1. Monthly sums (A) and cumulative NEE (B) before (solid lines) and after (dashed lines) the directional heterogeneity correction (Hadden and Grelle, 2017).

https://doi.org/10.5194/egusphere-2022-384
Preprint. Discussion started: 9 June 2022
© Author(s) 2022. CC BY 4.0 License.

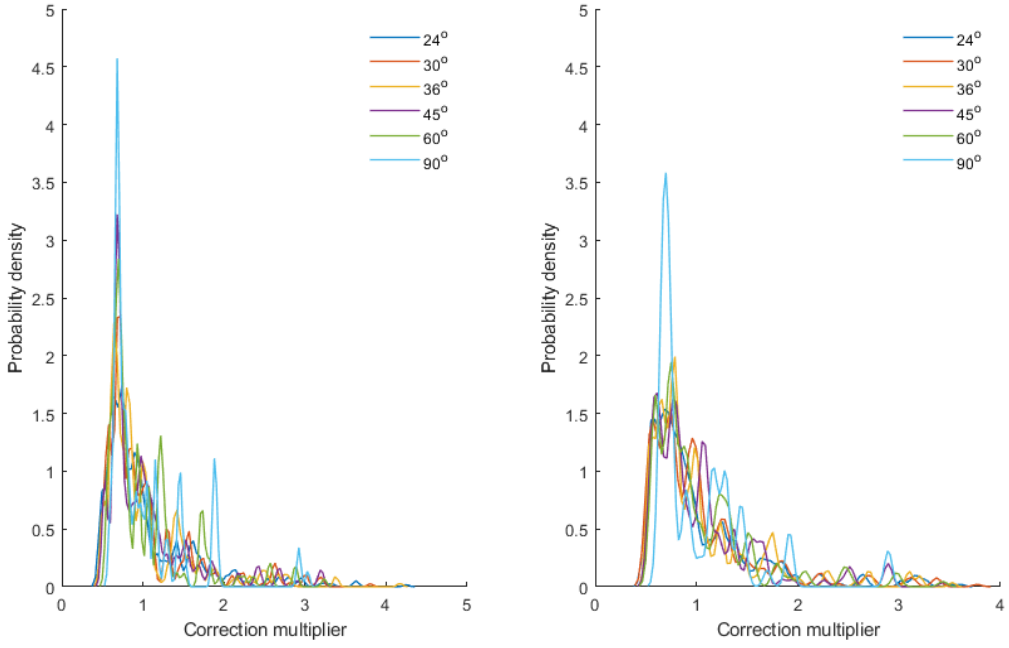

Figure A2. The probability density function of directional heterogeneity correction multipliers calculated for different sizes of wind direction vectors for NEE30 (left panel) and NEE70 (right panel).

660

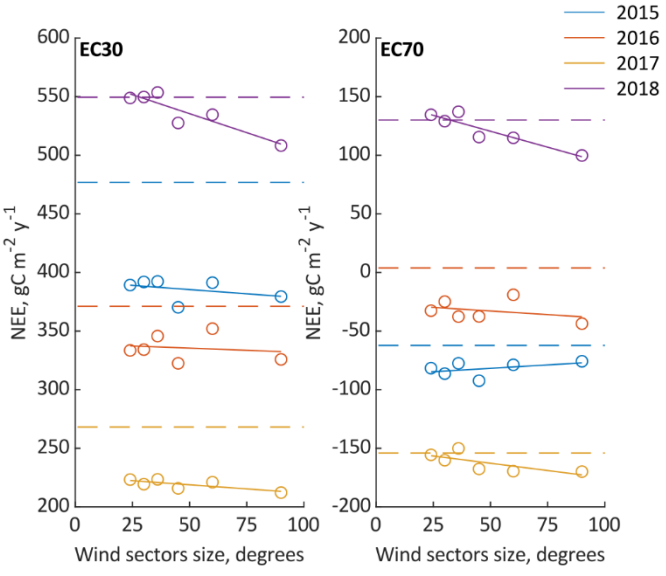

Figure A3. Annual sums of NEE from EC30 (A) and EC70 (B). Dashed lines represent annual sums without the directional heterogeneity correction. Filled markers represent annual NEE if 45º wind sectors were chosen following the original method (Hadden and Grelle, 2017)

https://doi.org/10.5194/egusphere-2022-384
Preprint. Discussion started: 9 June 2022
© Author(s) 2022. CC BY 4.0 License.

665

Table A1. Bonferroni adjusted p-values of Kruskal-Wallis test performed on daily sums of NEE, ER and GPP from EC30 and EC70 systems, each month separately. Statistically significant differences (p<0.05) are marked in bold.

Year	*Month*	*p (NEE)*	*p (GPP)*	*p (ER)*
2015	1	>0.1	0.04617	>0.1
2015	2	>0.1	>0.1	>0.1
2015	3	>0.1	>0.1	>0.1
2015	4	>0.1	>0.1	0.0793
2015	5	>0.1	3.254e-05	2.099e-07
2015	6	9.266e-05	3.254e-05	2.099e-07
2015	7	2.573e-07	0.0001681	1.194e-07
2015	8	1.724e-05	0.07199	9.694e-07
2015	9	4.531e-06	0.0003123	2.803e-08
2015	10	>0.1	0.04391	0.01312
2015	11	0.0005797	>0.1	0.04003
2015	12	0.001526	0.09154	3.103e-05
2016	1	>0.1	0.00996	>0.1
2016	2	>0.1	0.003186	2.161e-05
2016	3	>0.1	5.984e-06	3.915e-07
2016	4	>0.1	0.002957	>0.1
2016	5	>0.1	0.001191	1.486e-05
2016	6	>0.1	0.0003348	4.255e-07
2016	7	>0.1	0.001191	3.207e-08
2016	8	4.393e-06	0.00018	1.846e-09
2016	9	0.00113	0.01324	0.0003845
2016	10	0.0002696	>0.1	>0.1
2016	11	>0.1	>0.1	>0.1
2016	12	>0.1	>0.1	>0.1
2017	1	>0.1	>0.1	>0.1
2017	2	>0.1	>0.1	>0.1
2017	3	>0.1	>0.1	>0.1
2017	4	>0.1	>0.1	>0.1

https://doi.org/10.5194/egusphere-2022-384
Preprint. Discussion started: 9 June 2022
© Author(s) 2022. CC BY 4.0 License.

2017	5	>0.1	>0.1	>0.1
2017	6	>0.1	1.187e-05	2.057e-09
2017	7	>0.1	4.747e-06	9.442e-10
2017	8	1.574e-06	0.0007658	3.045e-07
2017	9	4.255e-07	0.0002359	3.898e-07
2017	10	>0.1	0.01242	>0.1
2017	11	0.0009904	0.04945	0.01402
2017	12	1.847e-06	7.857e-05	4.747e-06
2018	1	0.04391	>0.1	>0.1
2018	2	>0.1	0.0008448	>0.1
2018	3	>0.1	6.462e-06	0.007525
2018	4	>0.1	>0.1	>0.1
2018	5	>0.1	0.005342	0.006718
2018	6	>0.1	2.395e-05	5.512e-09
2018	7	0.002638	4.064e-06	1.145e-09
2018	8	6.439e-07	9.038e-05	5.929e-07
2018	9	1.303e-06	0.0001907	2.099e-07
2018	10	>0.1	0.001623	1.379e-05
2018	11	0.0006203	>0.1	0.0001776
2018	12	4.573e-08	>0.1	2.683e-08

Table A2. The influence of a wind sector size in the directional heterogeneity correction on the annual NEE in gC m^{-2} y^{-1}.

	24º	30º	36º	45º	60º	90º	Avg
EC30							
2015	-87.6 (18%)	-84.9 (18%)	-84.5 (18%)	-106.6 (22%)	-85.6 (18%)	-67.4 (20%)	-91.1 (19%)
2016	-37.7 (10%)	-36.9 (10%)	-25.4 (7%)	-48.7 (13%)	-19.1 (5%)	-45.3 (12%)	-35.6 (9%)
2017	-44.8	-48.7	-44.6	-52.3	-47.1	-55.9	-48.9

https://doi.org/10.5194/egusphere-2022-384
Preprint. Discussion started: 9 June 2022
© Author(s) 2022. CC BY 4.0 License.

	(17%)	(18%)	(17%)	(19%)	(17%)	(21%)	(18%)
2018	-0.6 (<1%)	+0.2 (<1%)	+4.0 (<1%)	-21.9 (4%)	-14.9 (3%)	-41.2 (8%)	-12.4 (3%)
Avg	-42.7 (10%)	-42.6 (10%)	-37.6 (9%)	-57.4 (14%)	-41.7 (10%)	-60.0 (14%)	
EC70							
2015	-19.4 (31%)	-24.1 (39%)	-15.3 (25%)	-30.15 (48%)	-16.6 (27%)	-13.6 (22%)	-19.8 (32%)
2016*	-36.4 (-)	-28.7 (-)	-41.5 (-)	-41.4 (-)	-22.9 (-)	-47.5 (-)	-36.4 (-)
2017	-1.6 (1%)	-6.2 (4%)	+3.9 (3%)	-13.6 (9%)	-15.5 (10%)	-15.9 (10%)	-8.1 (5%)
2018	+4.5 (4%)	-1.0 (<1%)	+7.0 (5%)	-14.5 (11%)	-15.2 (12%)	-30.3 (23%)	-8.2 (6%)
Avg	-13.2 (64%)	-15.0 (73%)	-11.5 (56%)	-24.9 (121%)	-17.6 (85%)	-26.8 (130%)	

* the correction changed the sign of NEE from positive to negative, so no percent change is reported